Sparsity-Based Joint NBI and Impulse Noise Mitigation in Hybrid PLC-Wireless Transmissions

Mahmoud Elgenedy*, Mohamed Mokhtar†, Ridha Hamila‡, Waheed U. Bajwa§, Ahmed S. Ibrahim¶ and Naofal Al-Dhahir*
* University of Texas at Dallas, Richardson, TX, USA, Emails: {mahmoud.elgenedy, aldhahir}@utdallas.edu
† Interdigital Inc, Conshohocken, PA, USA, Email: mohamed.awadin@interdigital.com
‡ Qatar University, Doha, Qatar, Email: hamila@qu.edu.qa
§ Rutgers, The State University of New Jersey, Piscataway, NJ, USA, Email: waheed.bajwa@rutgers.edu
¶ Florida International University, Miami, FL, USA, Email: aibrahim@fiu.edu

***Abstract*—We propose a new sparsity-aware framework to model and mitigate the joint effects of narrow-band interference (NBI) and impulsive noise (IN) in hybrid powerline and unlicensed wireless communication systems. The proposed mitigation techniques, based on the principles of compressive sensing (CS), exploit the inherent (non-contiguous or contiguous) sparse structures of NBI and IN in the frequency and time domains, respectively. For the non-contiguous NBI and IN, we develop a multi-level orthogonal matching pursuit recovery algorithm that exploits prior knowledge about the sparsity level at each receive antenna and powerline to further reduce computational complexity without performance loss. In addition, for the non-contiguous asynchronous NBI scenario, we investigate the application of time-domain windowing to enhance the NBI's sparsity and, hence, improve the NBI mitigation performance. For the contiguous NBI and IN scenario, we estimate the NBI and IN signals by modeling their burstiness as block-sparse vectors with and without prior knowledge of the bursts' boundaries. Moreover, we show how to exploit the spatial correlations of the NBI and IN across the receive antennas and powerlines to convert a non-contiguous NBI and IN problem to a block-sparse estimation problem with much lower complexity. Furthermore, we investigate a Bayesian linear minimum mean square error based approach for estimating both non-contiguous and contiguous NBI and IN based on their second-order statistics to further improve the estimation performance. Finally, our numerical results illustrate the superiority of the joint processing of our proposed NBI and IN sparsity-based mitigation techniques compared to separate processing of the wireless and powerline received signals.**

I. Introduction

To enhance the broadband transmission reliability and/or increase the coverage area, there has been an increased recent focus in realizing additional diversity dimensions from simultaneous transmissions over multiple physical layers. Wireless communication in the unlicensed frequency bands and powerline communication (PLC) are attractive candidates for achieving this goal due to their ubiquity [3]–[7].

Broadband PLC standards such as IEEE P1901.1 [8] and ITU-T G.hn [9] adopt orthogonal frequency division multiplexing (OFDM) in the 1.8–250 MHz frequency band. Broadband wireless local area network (WLAN) standards such as IEEE 802.11n also adopt OFDM in the 2.4 GHz and/or 5 GHz unlicensed frequency bands. To enhance communication reliability, a hybrid PLC-wireless communication system simultaneously transmits OFDM symbols over the PLC and WLAN channels followed by joint processing of both received signals to exploit the independence of the interference and channels characteristics of the two physical media. Unlike channel fading and interference in receive-diversity-based wireless communication systems which typically follow the same statistical distributions on all receive branches, channel fading and interference distributions are different for the PLC and wireless receive branches. However, a hybrid PLC-wireless system faces the following two main challenges. First, in-home PLC systems suffer from impulsive noise (IN) because of sudden voltage changes caused by on-off switching of in-home appliances and power electronics devices such as silicon-controlled rectifiers, switching regulators, and brush motors [10]. Second, WLAN transmissions are subject to narrow-band interference (NBI) from other wireless communication signals in the same frequency band including cordless phones and Bluetooth devices [11]. Our main objective in this paper is to investigate novel approaches for joint NBI and IN mitigation in OFDM-based hybrid PLC-wireless transmissions by exploiting the inherent sparsity of the NBI and IN signals in the frequency and time domains, respectively.

Considering earlier works, hybrid wireless and PLC systems are studied in [3]–[6] for broadband communications and in [7], [12]–[16] for narrowband communications. In [3]–[5], the performance of maximum ratio combining, selection combining and other receiver combining schemes are analyzed. Both [4] and [5] assume that the noise in the PLC link follows a Middleton Class-A model and the noise in the wireless link is additive white Gaussian noise (AWGN), while the authors of [3] assume that the noise in both the PLC and wireless links is AWGN. Using relaying in wireless and PLC networks is investigated in [6] under the AWGN model for the wireless link. In [7], the noise on the PLC link is modeled as a mixture of synchronous and asynchronous impulse noise while a Gaussian mixture noise model is adopted for the wireless link. In [12]–[16], the noise on the PLC link is modeled as a cyclostationary random process [17]–[19] while the Gaussian mixture noise model is used for the wireless link. None of these papers exploited the NBI and IN sparsity over different domains to estimate and mitigate their performance-limiting effects.

NBI and IN Mitigation in OFDM systems was investigated in [11], [20] which exploit the NBI and IN sparsity to mitigate their effects based on sparsity-based techniques. They showed that sparsity-based NBI or IN mitigation techniques

This work is supported by NPRP grant # NPRP 8-627-2-260 from the Qatar National Research Fund (a member of Qatar Foundation). Parts of this work appeared in [1], [2]. The statements made herein are solely the responsibility of the authors.

outperforms the traditional interference mitigation techniques. However, they did not study the joint mitigation of NBI and IN.

Building on our initial findings in [1], [2], in this paper, we exploit additional features of the NBI and IN signals and apply sparse recovery algorithms that lead to significant performance improvements. Our main contributions are:

- We develop a novel sparsity-based framework to jointly mitigate non-contiguous and contiguous NBI and IN in hybrid PLC-wireless communication systems by exploiting the NBI and IN inherent sparsity in the time and frequency domains.
- We utilize prior knowledge of the sparsity level across different receive ports and propose a multi-level orthogonal matching pursuit (OMP) algorithm for non-contiguous NBI and IN signals.
- To improve the estimation accuracy of asynchronous NBI, we apply a time-domain windowing to the received signal to enhance the asynchronous NBI sparsity.
- We investigate sparsity-based mitigation algorithms under different assumptions that exploit the bursty structure of contiguous NBI and IN for NBI and IN estimation. Assuming known bursts' boundaries (block sparse case[1]), we investigate the use of the block orthogonal matching pursuit (BOMP) algorithm [21]. Without this knowledge, we study another sparsity-based mitigation algorithm which was proposed in [22].
- We exploit prior knowledge of NBI and IN second-order statistics and quantify the performance gains of a Bayesian linear minimum mean square error estimator (LMMSE) over the conventional least-squares estimator for contiguous and non-contiguous NBI and IN.
- We exploit the spatial correlation across the receive ports (either antennas or wires) for the wireless or PLC links to convert the non-contiguous NBI and IN recovery problem to a block sparse signal recovery problem. Then, we propose a multi-level BOMP recovery algorithm for the case of different NBI and IN burst sizes. The proposed multi-level BOMP algorithm is less complex and enjoys a performance advantage over the OMP algorithm.
- We compare the NBI and IN mitigation performance in the case of joint and separate processing of PLC and wireless received signals and demonstrate the superiority of the former over the latter for a wide span of NBI and IN power levels.

Note that the first and third contributions above were discussed in [2], while the fourth contribution above was discussed in [1]. All other contributions were not investigated in [1] and [2].

Notation: Lower-case bold letters denote vectors and upper-case bold letters denote matrices. In addition, $\mathbf{I}$ and $\mathbf{F}$ denote the identity and the unitary discrete Fourier transform (DFT) matrices, respectively, while subscripts denote their dimensions. Matrices/vectors in the frequency domain are denoted by $\mathbf{A}_X^{(u)}/\mathbf{a}_X^{(u)}$, where the subscript $X \in \{W, P\}$ denotes the communication system with W for wireless system and P for PLC system, while the superscript u denotes the u^{th} antenna/wire. The corresponding time domain matrices/vectors are denoted by $\bar{\mathbf{A}}_X^{(u)}/\bar{\mathbf{a}}_X^{(u)}$. The operation diag$[\mathbf{v}]$ creates a square diagonal matrix with the elements of vector $\mathbf{v}$ on the main diagonal. Moreover, the operations $(\cdot)^H$, $(\cdot)^*$ and $(\cdot)^T$ denote the complex-conjugate transpose, complex-conjugate and transpose operations. Furthermore, the operations $\mathbb{E}[\cdot]$ and $|\cdot|$ denote the statistical expectation and absolute value operations. The l_0 norm of a vector $\mathbf{a}$ is denoted by $\|\mathbf{a}\|_0$ which counts the number of non-zero elements of the vector $\mathbf{a}$. Finally, $\|\mathbf{a}\|_1$ and $\|\mathbf{a}\|_2$ denote the l_1 norm and l_2 norm of the vector $\mathbf{a}$, respectively, while $\|\mathbf{A}\|$ denotes the spectral norm of the matrix $\mathbf{A}$ and is given by $\max_{\mathbf{x}:\mathbf{x}\neq 0} \|\mathbf{A}\mathbf{x}\|_2/\|\mathbf{x}\|_2$.

Paper Organization: Our system model, assumptions for hybrid PLC-wireless systems, and the problem formulation are defined in Section II. Our proposed sparsity-based approach for joint mitigation of *non-contiguous* NBI and IN is described in Section III, whereas our investigations on the extensions of the non-contiguous to asynchronous NBI, multi-level OMP and Basysian LMMSE based recovery algorithm are in Subsections III-C, III-A and III-B, respectively. In Section IV, we study *contiguous* NBI and IN estimation and mitigation for hybrid PLC-wireless systems. Extensions to unknown block boundaries, multi-level BOMP and Bayesian LMMSE block recovery are discussed in Subsections IV-A, IV-C and IV-B, respectively. Finally, simulation results and concluding remarks are given in Sections V and VI, respectively.

II. System Model

We assume single-input multiple-output (SIMO) OFDM simultaneous transmissions over wireless and PLC links [4] as shown in Fig. 1. The wireless link operates in the WLAN unlicensed frequency band and consists of a single-antenna transmitter and a K-antenna receiver. The PLC receiver can process up to $\beta \in \{1, 2, 3\}$ outputs over its 3 receive wires (phases). The NBI over the different wireless receive antennas is assumed to be uncorrelated. In addition, we assume that the PLC receive wires experience uncorrelated IN. Assuming uncorrelated NBI/IN over the different receive antennas/wires is a worst-case assumption since the spatial correlation between the wireless and/or PLC receive branches can be exploited to further enhance the NBI and IN mitigation performance, as will be discussed in Section IV-C. Given these assumptions, the received signals at the k^{th}, $k \in \{1, \ldots, K\}$, antenna and the j^{th}, $j \in \{1, \ldots, \beta\}$, wire are given by

$$\bar{\mathbf{y}}_W^{(k)} = \bar{\mathbf{H}}_W^{(k)} \bar{\mathbf{x}} + \bar{\mathbf{i}}_W^{(k)} + \bar{\mathbf{n}}_W^{(k)}, \tag{1}$$

$$\bar{\mathbf{y}}_P^{(j)} = \bar{\mathbf{H}}_P^{(j)} \bar{\mathbf{x}} + \bar{\mathbf{i}}_P^{(j)} + \bar{\mathbf{n}}_P^{(j)}, \tag{2}$$

Assuming M OFDM subcarriers per OFDM symbol, the $\bar{\mathbf{H}}_W^{(k)}$ and $\bar{\mathbf{H}}_P^{(j)}$ denote the $M \times M$ circulant channel matrices between the transmitter's antenna/wire and the $k^{\text{th}}/j^{\text{th}}$ receiver's antenna/wire of the wireless/PLC link. The first columns of these matrices are $\begin{bmatrix} \bar{\mathbf{h}}_W^{(k)T} & \mathbf{0}_{1\times M-L_W} \end{bmatrix}^T$ and $\begin{bmatrix} \bar{\mathbf{h}}_P^{(j)T} & \mathbf{0}_{1\times M-L_P} \end{bmatrix}^T$, where $\bar{\mathbf{h}}_W^{(k)}$ and $\bar{\mathbf{h}}_P^{(j)}$ are the wireless

[1]The term *bursts* is used in this paper when the bursts' boundaries are unknown, while the term *block* is used for the case of known bursts' boundaries.

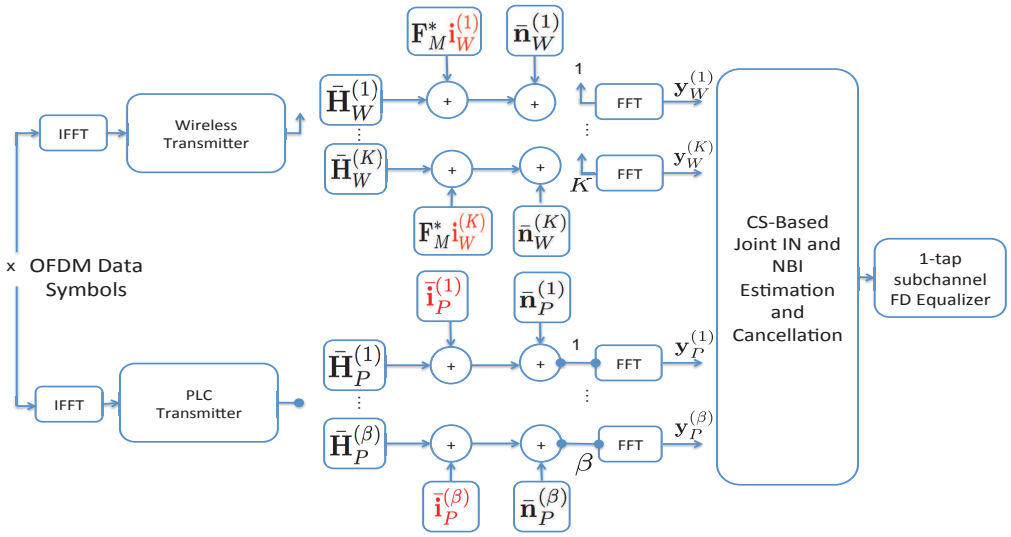

Fig. 1. System model of the SIMO hybrid wireless/PLC system (red fonts indicate sparse vectors).

and PLC channel impulse response (CIR) vectors with L_W and L_P taps, respectively. The wireless CIR taps is assumed to be Gaussian distributed, while the magnitudes of the PLC CIR taps are assumed log-normal distributed [3]. Furthermore, we assume perfect channel state information (CSI) at the wireless and PLC receivers. Using $\mathbf{x}$ for the $M \times 1$ OFDM data vector, the vector $\bar{\mathbf{x}}$ in (1) and (2) is defined as $\bar{\mathbf{x}} = \mathbf{F}_M^* \mathbf{x}$. Furthermore, $\bar{\mathbf{n}}_W^{(k)}$ and $\bar{\mathbf{n}}_P^{(j)}$ denote complex zero-mean circularly-symmetric AWGN vectors at the $k^{\text{th}}/j^{\text{th}}$ receiver's antenna/wire with variances σ_W^2 and σ_P^2, respectively. Finally, the NBI (sparse in the frequency domain) and the IN (sparse in the time domain) vectors at each antenna/wire are denoted by $\bar{\mathbf{i}}_W^{(k)}$ and $\bar{\mathbf{i}}_P^{(j)}$, respectively.

Applying the DFT to (1) and (2), we obtain

$$\underbrace{\mathbf{F}_M \bar{\mathbf{y}}_W^{(k)}}_{\triangleq \mathbf{y}_W^{(k)}} = \underbrace{\mathbf{F}_M \bar{\mathbf{H}}_W^{(k)} \mathbf{F}_M^*}_{\triangleq \Lambda_W^{(k)}} \mathbf{x} + \underbrace{\mathbf{F}_M \bar{\mathbf{i}}_W^{(k)}}_{\triangleq \mathbf{i}_W^{(k)}} + \underbrace{\mathbf{F}_M \bar{\mathbf{n}}_W^{(k)}}_{\triangleq \mathbf{n}_W^{(k)}}, \text{ and} \quad (3)$$

$$\underbrace{\mathbf{F}_M \bar{\mathbf{y}}_P^{(j)}}_{\triangleq \mathbf{y}_P^{(j)}} = \underbrace{\mathbf{F}_M \bar{\mathbf{H}}_P^{(j)} \mathbf{F}_M^*}_{\triangleq \Lambda_P^{(j)}} \mathbf{x} + \mathbf{F}_M \bar{\mathbf{i}}_P^{(j)} + \underbrace{\mathbf{F}_M \bar{\mathbf{n}}_P^{(j)}}_{\triangleq \mathbf{n}_P^{(j)}}, \quad (4)$$

where $\Lambda_W^{(k)}$ and $\Lambda_P^{(j)}$ are $M \times M$ diagonal matrices whose diagonal elements (collected in the vectors $\begin{bmatrix} h_{W,1}^{(k)} & \dots & h_{W,M}^{(k)} \end{bmatrix}$ and $\begin{bmatrix} h_{P,1}^{(j)} & \dots & h_{P,M}^{(j)} \end{bmatrix}$) are the channel frequency response (CFR) coefficients of the $k^{\text{th}}/j^{\text{th}}$ receiver's antenna/wire of the wireless/PLC output, respectively. The vector $\mathbf{i}_W^{(k)}$ denotes the frequency-domain (FD) NBI at the k^{th} antenna. In addition, the sparsity of NBI (in frequency) and IN (in time) implies that $\|\mathbf{i}_W^{(k)}\|_0 \triangleq \rho_W^{(k)} \ll M$ and $\|\bar{\mathbf{i}}_P^{(j)}\|_0 \triangleq \rho_P^{(j)} \ll M$.

Combining the received wireless and PLC signals in (3) and (4) for all $k \in \{1, \dots, K\}$ and $j \in \{1, \dots, \beta\}$ into a single column vector leads to the following model

$$\underbrace{\begin{bmatrix} \mathbf{y}_W^{(1)} \\ \vdots \\ \mathbf{y}_W^{(K)} \\ \mathbf{y}_P^{(1)} \\ \vdots \\ \mathbf{y}_P^{(\beta)} \end{bmatrix}}_{\triangleq \mathbf{y}} = \underbrace{\begin{bmatrix} \Lambda_W^{(1)} \\ \vdots \\ \Lambda_W^{(K)} \\ \Lambda_P^{(1)} \\ \vdots \\ \Lambda_P^{(\beta)} \end{bmatrix}}_{\triangleq \mathbf{G}} \mathbf{x} + \underbrace{\begin{bmatrix} \mathbf{i}_W^{(1)} \\ \vdots \\ \mathbf{i}_W^{(k)} \\ \mathbf{F}_M \bar{\mathbf{i}}_P^{(1)} \\ \vdots \\ \mathbf{F}_M \bar{\mathbf{i}}_P^{(\beta)} \end{bmatrix}}_{\triangleq \mathbf{i}} + \underbrace{\begin{bmatrix} \mathbf{n}_W^{(1)} \\ \vdots \\ \mathbf{n}_W^{(K)} \\ \mathbf{n}_P^{(1)} \\ \vdots \\ \mathbf{n}_P^{(\beta)} \end{bmatrix}}_{\triangleq \mathbf{n}}. \quad (5)$$

Here, we refer to the $M(K+\beta) \times 1$ vector $\mathbf{y}$ as the *measurement vector*, while we refer to the $M(K+\beta) \times M$ matrix $\mathbf{G}$ as the *channel matrix*. Note that $\mathbf{G}$ consists of the CFR matrices of the wireless and PLC links, i.e., $\mathbf{G} \triangleq \begin{bmatrix} \mathbf{G}_W^H & \mathbf{G}_P^H \end{bmatrix}^H$, where $\mathbf{G}_W$ and $\mathbf{G}_P$ denote the concatenated FD channel matrices for the wireless and PLC links, respectively. Finally, $\mathbf{i}$ denotes the $M(K+\beta) \times 1$ combined NBI and IN vectors, $\mathbf{n}$ is the equivalent $M(K+\beta) \times 1$ noise vector in frequency domain. Our main objective here is to use (5) to estimate the NBI and IN vectors.

In practice, the NBI and IN signals inherit several attractive features due to the nature of wireless and PLC links, respectively, that play an important role in mitigating their effects. Specifically, both NBI and IN can either be non-contiguous or contiguous, i.e., they can occupy either dispersed or consecutive frequency subcarriers and time samples, respectively. Moreover, NBI can be synchronous or asynchronous depending on the interference source. In the synchronous scenario, the NBI samples fall exactly on the desired signal's DFT grid while asynchronous NBI exhibits a carrier frequency offset with respect to the desired signal's carrier frequency. In this paper, we mainly focus on the synchronous NBI and IN case. The asynchronous NBI is only discussed in Subsection III-C. Consideration of asynchronous IN is beyond the scope of this paper. In the next sections, we propose efficient algorithms to effectively exploit NBI and IN signal features.

III. Sparsity-Based Joint Estimation of Non-Contiguous NBI and IN

In this section, we investigate the use of sparse recovery algorithms for the mitigation of non-contiguous NBI and synchronous IN signals. Initially, we assume synchronous NBI, then we discuss the asynchronous NBI case in Subsection III-C. To estimate NBI and IN vectors from $\mathbf{y}$, we first cancel the unknown term $\mathbf{Gx}$ in (5) by projecting $\mathbf{y}$ onto the left-null space of $\mathbf{G}$ using the projection matrix [11], [20] $\mathbf{Q} = \mathbf{I}_{M(K+\beta)} - \mathbf{G}\mathbf{G}^{\dagger}$, where $\mathbf{G}^{\dagger}$ denotes the pseudoinverse of $\mathbf{G}$ given by $\left(\mathbf{G}^H\mathbf{G}\right)^{-1}\mathbf{G}^H$ for the case of a full column rank $\mathbf{G}$. Since $\mathbf{QG} = \mathbf{0}_{M(K+\beta)\times M}$, the projected received signal is given by

$$\mathbf{y}' \triangleq \mathbf{Qy} = \mathbf{Qi} + \mathbf{Qn}. \tag{6}$$

Let $\mathbf{i}_{\text{eqv}}$ represent the concatenation of the NBI vector in the frequency domain and IN vector in the time domain, i.e., $\mathbf{i}_{\text{eqv}} \triangleq \begin{bmatrix} \mathbf{i}_W^{(1)^T} & \dots & \mathbf{i}_W^{(K)^T} & \bar{\mathbf{i}}_P^{(1)^T} & \dots & \bar{\mathbf{i}}_P^{(\beta)^T} \end{bmatrix}^T$. Then, vector $\mathbf{i}$ can be written in terms of $\mathbf{i}_{\text{eqv}}$ as follows

$$\mathbf{i} = \underbrace{\begin{bmatrix} \mathbf{I}_{KM} & \mathbf{0}_{KM\times\beta M} \\ \mathbf{0}_{\beta M\times KM} & \mathbf{I}_\beta \otimes \mathbf{F}_M \end{bmatrix}}_{\triangleq\mathbf{A}} \mathbf{i}_{\text{eqv}}, \tag{7}$$

where $\otimes$ denotes the Kronecker product operation.

Now, (6) can be rewritten as follows

$$\mathbf{y}' \triangleq \mathbf{Q}_{\text{eqv}}\mathbf{i}_{\text{eqv}} + \mathbf{n}', \tag{8}$$

where the *measurement matrix* $\mathbf{Q}_{\text{eqv}}$ is defined in terms of $\mathbf{Q}$ as $\mathbf{Q}_{\text{eqv}} = \mathbf{QA}$, and $\mathbf{n}' \triangleq \mathbf{Qn}$. Now, we have reduced our joint NBI and IN estimation problem to the linear model in (8). While we can use conventional estimation techniques in this setting to estimate $\mathbf{i}_{\text{eqv}}$, we know from [11], [20], [23] that exploiting the sparsity of $\mathbf{i}_{\text{eqv}}$ can further enhance the estimation performance. In particular, CS principles advocate for the estimation of sparse vectors by solving problems of the form (8) as follows

$$\hat{\mathbf{i}}_{\text{eqv}} \triangleq \underset{\mathbf{i}\in\mathbb{C}^{(K+\beta)M}}{\operatorname{argmin}} \|\mathbf{Q}_{\text{eqv}}\mathbf{i} - \mathbf{y}'\|_2^2 \;\text{ subject to }\; \|\mathbf{i}\|_0 = S, \tag{9}$$

where S is the number of non-zero elements of $\mathbf{i}_{\text{eqv}}$, defined as $S \triangleq \sum_{k=1}^{K}\rho_W^{(k)} + \sum_{j=1}^{\beta}\rho_P^{(j)}$.

Note that while (9) in its stated form has combinatorial complexity, there exist a number of greedy and optimization-based techniques in the CS literature that can be applied to efficiently solve this problem. In this paper, we use a well-known greedy algorithm, named *orthogonal matching pursuit* (OMP) [24], because of its low computational complexity. OMP algorithm estimates $\hat{\mathbf{i}}_{\text{eqv}}$ iteratively by selecting S columns of $\mathbf{Q}_{\text{eqv}}$ that are most correlated with the observations $\mathbf{y}'$ and then solving a *restricted* least-squares (LS) problem using the selected columns. For completeness, we summarize its main steps in Algorithm 1 using the notation of this paper.

Remark: The matrix $\mathbf{Q}_{\text{eqv}}$ has a closed-form expression since both $\mathbf{Q}$ and $\mathbf{G}$ have a special structure and can be decomposed into diagonal matrices. Specifically, after some algebraic manipulations, it follows that

$$\mathbf{Q} = \mathbf{I}_{M(K+\beta)} - \begin{bmatrix} \mathbf{G}_W\mathbf{G}_W^H & \mathbf{G}_W\mathbf{G}_P^H \\ \mathbf{G}_P\mathbf{G}_W^H & \mathbf{G}_P\mathbf{G}_P^H \end{bmatrix} \times (\mathbf{I}_{K+\beta}\otimes\Psi) \tag{10}$$

with the matrix Ψ defined as follows:

$$\Psi \triangleq \Big[\Lambda_W^{(1)}\left(\Lambda_W^{(1)}\right)^H + \dots + \Lambda_W^{(K)}\left(\Lambda_W^{(K)}\right)^H + \Lambda_P^{(1)}\left(\Lambda_P^{(1)}\right)^H + \dots + \Lambda_P^{(\beta)}\left(\Lambda_P^{(\beta)}\right)^H\Big]^{-1}. \tag{11}$$

Assuming perfect CSI, $\mathbf{Q}$ can be computed efficiently from (10) since it is much easier to compute the inverse of the diagonal matrix in (11), denoted by Ψ, instead of using the form $\mathbf{Q} = \mathbf{I}_{M(K+\beta)} - \mathbf{G}\mathbf{G}^{\dagger}$ which requires computation of the inverse of the general matrix $\left(\mathbf{G}^H\mathbf{G}\right)^{-1}$.

In the following, our proposed framework for joint estimation of non-contiguous NBI and IN is extended to include the following cases. First, in Subsection III-A, we consider the general case of unequal sparsity levels of NBI and IN on different antennas/wires. Second, in Subsection III-B, we exploit knowledge of the second order statistics of the NBI and IN to enhance the estimation quality. Finally, in Subsection III-C, we investigate the case when the carrier frequency of the NBI signal is different than the desired signal's carrier frequency (asynchronous NBI), which leads to NBI leakage across the OFDM subcarriers.

Algorithm 1 OMP for Joint Estimation of Non-Contiguous NBI and IN

Inputs: Matrix $\mathbf{Q}_{\text{eqv}}$, vector $\mathbf{y}'$, and sparsity level S.
Initialization: Define set index $I_0 = \{\}$, set residual $\mathbf{r}_0 = \mathbf{y}'$, estimate $\hat{\mathbf{i}}_{\text{eqv}} = \mathbf{0}_{(K+\beta)M}$, and the iteration count $l = 1$.
The l^{th} iteration:

1) Calculate $\delta_i = \left|\mathbf{r}_{l-1}^H\mathbf{Q}_{\text{eqv}}(:,i)\right|$ for all $i \notin I_{l-1}$, where $\mathbf{Q}_{\text{eqv}}(:,i)$ denotes the column i in the matrix $\mathbf{Q}_{\text{eqv}}$.
2) Search for index of the next non-zero entry at the l^{th} iteration as $c_l = \underset{i}{\operatorname{argmax}}\ \delta_i$.
3) Update the non-zero entries indices as $I_l = I_{l-1}\cup\{c_l\}$.
4) Set $\hat{\mathbf{i}}_{\text{eqv}}(I_l) = \left(\mathbf{Q}_{\text{eqv}}(:,I_l)\right)^{\dagger}\mathbf{y}'$, where $\hat{\mathbf{i}}_{\text{eqv}}(I_l)$ denotes the entries of $\hat{\mathbf{i}}_{\text{eqv}}$ indexed by I_l.
5) Calculate the residual error term at the l^{th} iteration as $\mathbf{r}_l = \mathbf{y}' - \mathbf{Q}_{\text{eqv}}(:,I_l)\hat{\mathbf{i}}_{\text{eqv}}(I_l)$.
6) **If** $l = S$ then exit, **else** set $l = l+1$ and go to Step 1.

A. Multi-Level OMP

In this subsection, we exploit knowledge of the, generally unequal, sparsity levels of the NBI and IN signals across antennas and wires, respectively. In this case, the problem formulation in (9) can be rewritten as follows:

$$\hat{\mathbf{i}}_{\text{eqv}} \triangleq \underset{\mathbf{i}\in\mathbb{C}^{(K+\beta)M}}{\operatorname{argmin}} \|\mathbf{Q}_{\text{eqv}}\mathbf{i} - \mathbf{y}'\|_2^2 \quad \text{subject to } \|\mathbf{T}_X^{(u)}\mathbf{i}\|_0 = \rho_X^{(u)},\ \forall(X,u), \tag{12}$$

where $(X,u) \in \{(W,1),...,(W,K),(P,1),...,(P,\beta)\}$, $\mathbf{T}_X^{(u)}$ is a diagonal matrix of size $(K+\beta)M \times (K+\beta)M$ and its

diagonal entries are all zeros except for M ones corresponding to the u^{th} receive antenna/wire. Hence, the operation $\|\mathbf{T}_X^{(u)}\mathbf{i}\|_0$ counts the number of non-zero entries in the NBI/IN vector at the u^{th} receive port.

To solve this problem, we present a modified version of the greedy OMP algorithm such that a multi-level sparsity constraint for each segment of vector $\mathbf{i}$ is satisfied. The modified multi-level OMP recovery algorithm aims to reduce computational complexity by reducing the search space based on the pre-defined different antennas'/wires' sparsity levels $\rho_X^{(u)}$. In other words, multi-level OMP aims to achieve the same performance as that of the greedy OMP at a much lower complexity. Specifically, we define the vector $z_X^{(u)}$ that counts the number of detected non-zero elements for each antenna/wire u for every iteration l. In each iteration l, we map the detected element index c_l to the corresponding antenna/wire u and update the vector $z_X^{(u)}$. Then, we compare the updated vector $z_X^{(u)}$ with the desired sparsity level $\rho_X^{(u)}$. Once the vector $z_X^{(u)}$ reaches the sparsity level for a specific antenna/wire u', i.e., $z_X^{(u')} = \rho_X^{(u')}$, we exclude all indices associated with the antenna/wire u' from the search space. The entire procedure for multi-level OMP is given in Algorithm 2.

Algorithm 2 Multi-level OMP for Joint Estimation of Non-Contiguous NBI and IN

Inputs: Vector $\mathbf{y}'$, matrix $\mathbf{Q}_{\text{eqv}}$, multi-level sparsity constraints $\rho_X^{(u)}$, and overall sparsity S.

Initialization: Define set index $I_0 = \tilde{I}_0 = \{\}$, set residual $\mathbf{r}_0 = \mathbf{y}'$, estimate $\hat{\mathbf{i}}_{\text{eqv}} = \mathbf{0}_{(K+\beta)M}$, iteration count $l = 1$, and $z_X^{(u)} = 1$, $(X, u) \in \{(W,1), ..., (W,K), (P,1), ..., (P,\beta)\}$.

The l^{th} iteration:

1) Compute $\delta_i = \left|\mathbf{r}_{l-1}^H \mathbf{Q}_{\text{eqv}}(:,i)\right|$ for all $i \notin \tilde{I}_{l-1}$.
2) Search for index of the next non-zero entry at the l^{th} iteration as $c_l = \underset{i}{\text{argmax}}\ \delta_i$.
3) **If** $c_l > MK$, **then** $X = P$ and $u = \left\lceil \frac{c_l - MK}{M} \right\rceil$, **else** $X = W$ and $u = \left\lceil \frac{c_l}{M} \right\rceil$.
4) For (X, u) calculated in the previous step, **if** $z_X^{(u)} > \rho_X^{(u)}$, **then** add all the column indices associated with the u^{th} receive port to the set $\tilde{I}_l$ if they do not exist already, i.e., $\tilde{I}_l = \tilde{I}_{l-1} \cup \psi$, where $\psi = \{(u-1)M + 1, ..., uM\}$ if $X = W$, and $\psi = \{((u-1)M + 1, ..., uM) + MK\}$ if $X = P$, and go to Step 1, **else** proceed to Step 5.
5) Update the non-zero elements indices as $I_l = I_{l-1} \cup \{c_l\}$ and $\tilde{I}_l = \tilde{I}_{l-1} \cup \{c_l\}$.
6) Set $\hat{\mathbf{i}}_{\text{eqv}}(I_l) = \left(\mathbf{Q}_{\text{eqv}}(:, I_l)\right)^{\dagger} \mathbf{y}'$, where $\hat{\mathbf{i}}_{\text{eqv}}(I_l)$ denotes the elements of $\hat{\mathbf{i}}_{\text{eqv}}$ indexed by I_l.
7) Calculate the residual error at the l^{th} iteration as $\mathbf{r}_l = \mathbf{y}' - \mathbf{Q}_{\text{eqv}}(:, I_l)\mathbf{i}_{\text{eqv}}(I_l)$ and set $z_X^{(u)} = z_X^{(u)} + 1$.
8) **If** $l = S$ then exit, **else** set $l = l + 1$ and go to Step 1.

Computational savings in multi-level OMP: We compare the total computational complexity of the multi-level OMP algorithm against the total computational complexity of the OMP algorithm in terms of the number of multiplications. As shown in Algorithm 1, for the OMP algorithm, a matrix/vector multiplication is required in Steps 1, 4 and 5. The first step of the OMP algorithm requires multiplying the vector $\mathbf{r}_{l-1}$ by the matrix $\mathbf{Q}_{\text{eqv}}(:,i)$, which is a subset of the matrix $\mathbf{Q}_{\text{eqv}}$ that includes all columns except the indices corresponding to the detected interference indices, i.e., $i \notin I_{l-1}$. To compute the LS estimate $\hat{\mathbf{i}}_{\text{eqv}}(I_l)$, Step 4 requires computation of the pseudo-inverse of $\mathbf{Q}_{\text{eqv}}(:, I_l)$ in addition to a matrix/vector multiplication, where $\mathbf{Q}_{\text{eqv}}(:, I_l)$ is a subset of the matrix $\mathbf{Q}_{\text{eqv}}$ that includes the columns corresponding only to the detected interference indices I_l. In Step 5, a matrix/vector multiplication between the estimated interference vector $\hat{\mathbf{i}}_{\text{eqv}}(I_l)$ and the matrix $\mathbf{Q}_{\text{eqv}}(:, I_l)$ is needed to compute the residual vector $\mathbf{r}_l$. Here, the computational complexity of Step 5 can be neglected since the vector $\hat{\mathbf{i}}_{\text{eqv}}(I_l)$ is a sparse vector with maximum sparsity level S. Moreover, in Step 4, $\mathbf{Q}_{\text{eqv}}(:, I_l)$ has a maximum dimension of $M(K+\beta) \times S$ in the last iteration. This means that, in the worst case, the LS estimation first requires inversion of a matrix of size $S \times S$ (which requires $S^3/3$ multiplications using Cholesky factorization) and then a matrix/vector multiplication requiring $M(K+\beta) \times S$ multiplications. Hence, under the assumption $S << M(K+\beta)$, the LS complexity is very small and can be neglected compared to the complexity of Step 1, which involves a matrix/vector multiplication requiring $M(K+\beta) \times M(K+\beta)$ multiplications. Similarly, for the multi-level OMP algorithm, the complexity is dominated by Step 1 under the assumption $S << M(K+\beta)$. Therefore, in the following computational complexity comparison, we focus only on the complexity of Step 1.

For simplicity, we assume the same sparsity level for all antennas and wires, i.e., $\rho_W^{(k)} = \rho_P^{(j)} = \rho$ for all $k \in \{1, ..., K\}$ and $j \in \{1, ..., \beta\}$. Now, let $N = M(K+\beta)$, then the total complexity of the OMP algorithm $\mathbb{C}_{OMP}$ can be expressed as follows:

$$\mathbb{C}_{OMP} = \sum_{i=0}^{S-1} N(N-i) = \sum_{m=1}^{K+\beta} \sum_{i=0}^{\rho-1} N(N-(m-1)\rho - i). \tag{13}$$

As discussed earlier, the computational savings for the multi-level OMP algorithm comes from the reduction of the search space (number of columns) in Step 1 with successive iterations. In particular, unlike the OMP algorithm, instead of eliminating one column every iteration, the multi-level OMP either eliminates one column or M columns in every iteration based on a condition on the number of detected NBI/IN subcarriers/samples at each antenna/wire. Since the complexity reduction in every iteration of the multi-level OMP is not deterministic, the complexity of the multi-level OMP is not fixed. Thus, we evaluate the best and worst case complexity for the multi-level OMP algorithm. For the best case complexity, the detection is performed for all NBI/IN indices associated with the first antenna/wire so that all columns corresponding to the first antenna/wire can be excluded from the remaining iterations, then the detection is performed for all NBI/IN indices associated with the following antenna/wire and so on. The complexity for the best case of the multi-level OMP

algorithm $\mathbb{C}_{MOMP,b}$ can be evaluated as follows:

$$\mathbb{C}_{MOMP,b} = \sum_{m=1}^{K+\beta} \sum_{i=0}^{\rho-1} N(N-(m-1)M-i). \quad (14)$$

Comparing (13) and (14), it is clear that the best case complexity of the multi-level OMP algorithm is much smaller than the complexity of the OMP algorithm since $M >> \rho$. However, the worst case complexity of the multi-level OMP algorithm occurs when the column's exclusion is not possible until the last $(K+\beta)$ iterations where every antenna/wire has only one remaining NBI/IN index to be detected. Since the complexity saving in the worst case multi-level OMP algorithm (compared to OMP algorithm) is only in the last $(K+\beta)$ iterations, the worst case complexity of the multi-level OMP algorithm $\mathbb{C}_{MOMP,w}$ as a function of the complexity of the OMP algorithm $\mathbb{C}_{OMP}$ is given by the following expression:

$$\mathbb{C}_{MOMP,w} = \mathbb{C}_{OMP} - \sum_{i=S-K-\beta+1}^{S-1} N(M-\rho)(i-S+K+\beta). \quad (15)$$

Note that the term subtracted from the $\mathbb{C}_{OMP}$ in (15) is always positive. Hence, the worst case complexity of the multi-level OMP algorithm is always lower than the complexity of the OMP algorithm. In Section V, we present numerical results for the computational complexity savings in the multi-level OMP compared to the OMP algorithm.

B. LMMSE Based OMP

In this subsection, we exploit knowledge of the second-order statistics of the NBI and IN signals, when they are available at the receiver, to further enhance the quality of their estimates. In particular, we propose replacing the LS estimator in Step 4 in Algorithm 1 (Step 6 in Algorithm 2) with the linear minimum mean square error (LMMSE) estimator based on the second-order statistics of NBI, IN and noise [25] as follows:

$$\hat{\mathbf{i}}_{\text{eqv}}(I_l) = \mathbb{E}\left[\mathbf{i}_{\text{eqv}}(I_l)\mathbf{y'}^H\right] \mathbb{E}\left[\mathbf{y'}\mathbf{y'}^H\right]^{-1} \mathbf{y'}, \quad (16)$$

where $\mathbb{E}\left[\mathbf{i}_{\text{eqv}}(I_l)\mathbf{y'}^H\right] = \mathbf{R}_{\mathbf{i}_{\text{eqv}}}\mathbf{Q}^H_{\text{eqv}}(:,I_l)$, $\mathbb{E}\left[\mathbf{y'}\mathbf{y'}^H\right] = \left(\mathbf{Q}_{\text{eqv}}(:,I_l)\mathbf{R}_{\mathbf{i}_{\text{eqv}}}\mathbf{Q}^H_{\text{eqv}}(:,I_l) + \mathbf{R}_{\mathbf{n'}}\right)$, and $\mathbf{R}_{\mathbf{i}_{\text{eqv}}}$ and $\mathbf{R}_{\mathbf{n'}}$ are the covariance matrices for $\mathbf{i}_{\text{eqv}}$ and $\mathbf{n'}$ in (8), respectively. For simplicity, we assume that the non-zero entries of the NBI and IN vectors are independent and identically distributed (i.i.d.) zero-mean Gaussian random variables with variances $\mathcal{E}_W$ and $\mathcal{E}_P$, respectively. In addition, we assume i.i.d. zero-mean Gaussian noise for both the wireless and PLC links with variances σ^2_W and σ^2_P, respectively.

To evaluate (16), we need to compute $\mathbf{R}_{\mathbf{i}_{\text{eqv}}}$ and $\mathbf{R}_{\mathbf{n'}}$. First, we derive an expression for $\mathbf{R}_{\mathbf{i}_{\text{eqv}}}$. Since both NBI and IN are assumed independent over different antennas/wires, $\mathbf{R}_{\mathbf{i}_{\text{eqv}}}$ is a block diagonal matrix and can be written as follows:

$$\mathbf{R}_{\mathbf{i}_{\text{eqv}}} = \text{diag}\left[\mathbf{R}^{(1)}_{\mathbf{i}_{\text{eqv},W}}, \cdots, \mathbf{R}^{(K)}_{\mathbf{i}_{\text{eqv},W}}, \mathbf{R}^{(1)}_{\mathbf{i}_{\text{eqv},P}}, \cdots, \mathbf{R}^{(\beta)}_{\mathbf{i}_{\text{eqv},P}}\right], \quad (17)$$

where each submatrix $\mathbf{R}^{(u)}_{\mathbf{i}_{\text{eqv},X}}$ can be evaluated as follows:

$$\mathbf{R}^{(u)}_{\mathbf{i}_{\text{eqv},X}} = \mathbb{E}\left[\mathbf{i}^{(u)}_{\text{eqv},X}\mathbf{i}^{(u)^H}_{\text{eqv},X}\right] = \sum_{\omega^u_X \in \mathfrak{U}^u_X} \mathbb{E}\left[\mathbf{i}^{(u)}_{\text{eqv},X}\mathbf{i}^{(u)^H}_{\text{eqv},X}|\omega^u_X\right] p(\omega^u_X). \quad (18)$$

Here, $\mathbf{i}^{(u)}_{\text{eqv},X} = \mathbf{i}^{(k)}_W$ when $X = W$, and $\mathbf{i}^{(u)}_{\text{eqv},X} = \bar{\mathbf{i}}^{(j)}_P$ when $X = P$. The summation in (18) is taken over the set of all possible sparsity profiles, denoted by $\mathfrak{U}^u_X$, while $p(\omega^u_X)$ is the probability that the ω^u_X sparsity profile is activated and it is assumed to be a uniform distribution[2], i.e.,

$$p(\omega^u_X) = \frac{1}{\binom{M}{\rho^{(u)}_X}}. \quad (19)$$

It is then straightforward to show that

$$\mathbf{R}^{(u)}_{\mathbf{i}_{\text{eqv},X}} = \mathcal{E}_X \frac{\binom{M-1}{\rho^{(u)}_X-1}}{\binom{M}{\rho^{(u)}_X}} \mathbf{I}_M = \mathcal{E}_X \frac{\rho^{(u)}_X}{M} \mathbf{I}_M. \quad (20)$$

Next, we evaluate the covariance matrix of the equivalent noise in (8), which is given by

$$\mathbf{R}_{\mathbf{n'}} = \mathbb{E}\left[\mathbf{n'}\mathbf{n'}^H\right] = \mathbf{Q}\mathbf{R}_{\mathbf{nn}}\mathbf{Q}^H, \quad (21)$$

where $\mathbf{R}_{\mathbf{nn}} = \text{diag}\left[\sigma^2_W \mathbf{I}_{KM}, \sigma^2_P \mathbf{I}_{\beta M}\right]$.

C. Joint Processing with Asynchronous NBI

In practice, the carrier frequency of the NBI signal can deviate from that of the desired signal which causes NBI energy leakage across the OFDM subcarriers, therefore, the sparsity level of the NBI is reduced. To improve the robustness of sparsity-based NBI recovery against carrier frequency offset (CFO), we apply time-domain windowing to reduce the DFT side lobes and enhance the sparsity level of the NBI signal. After applying the time-domain windowing to the wireless received signal and performing the DFT of (1), we get

$$\underbrace{\mathbf{F}_M\Phi\bar{\mathbf{y}}^{(k)}_W}_{\triangleq\check{\mathbf{y}}^{(k)}_W} = \underbrace{\mathbf{F}_M\Phi\bar{\mathbf{H}}^{(k)}_W\mathbf{F}^*_M}_{\triangleq\check{\Lambda}^{(k)}_W}\mathbf{x} + \underbrace{\mathbf{F}_M\Phi\mathbf{D}^{(k)}_W\bar{\mathbf{i}}^{(k)}_W}_{\triangleq\check{\mathbf{i}}^{(k)}_W} + \underbrace{\mathbf{F}_M\Phi\bar{\mathbf{n}}^{(k)}_W}_{\triangleq\check{\mathbf{n}}^{(k)}_W}, \quad (22)$$

where the matrix $\mathbf{D}^{(k)}_W \triangleq \text{diag}\left[1,\ \exp\left(i\frac{2\pi\alpha^{(k)}}{M}\right),\ \cdots,\ \exp\left(i\frac{2\pi\alpha^{(k)}(M-1)}{M}\right)\right]$ with $\alpha^{(k)}$ denoting the CFO between the NBI signal and the wireless received signal normalized to the OFDM subcarrier spacing. The CFO $\alpha^{(k)}$ is assumed to be uniformly-distributed in the range $[-0.5,\ 0.5]$, and i.i.d. across different antennas. The windowing matrix Φ is an $M \times M$ diagonal matrix where the diagonal elements are the window coefficients. Moreover, the matrix $\check{\Lambda}^{(k)}_W$ denotes the new $M \times M$ effective channel matrix after applying the windowing operation. Here, $\check{\mathbf{i}}^{(k)}_W$ denotes the FD NBI vector at the k^{th} receive antenna.

[2]Note that the assumptions on the NBI and IN statistical distributions are only required in this Subsection and Subsection IV-B to evaluate the covariance matrices. However, all other algorithms proposed in this paper are independent of NBI and IN statistical distributions assumptions.

The concatenated received wireless and PLC vector, denoted by $\check{\mathbf{y}}$, is given by

$$\check{\mathbf{y}} \triangleq \check{\mathbf{G}}\mathbf{x} + \check{\mathbf{i}} + \check{\mathbf{n}}, \tag{23}$$

where the *modified channel matrix* $\check{\mathbf{G}}$ is the same as $\mathbf{G}$ defined in (5) with $\Lambda_W^{(k)}$ replaced with $\check{\Lambda}_W^{(k)}$. In addition, the vector $\check{\mathbf{i}}$, which represents the combined NBI and IN vectors, is the same as $\mathbf{i}$ defined in (5) but $\mathbf{i}_W^{(k)}$ is replaced with $\check{\mathbf{i}}_W^{(k)}$. Similar to (8), we project $\check{\mathbf{y}}$ onto the left-null space of $\check{\mathbf{G}}$ using the projection matrix $\check{\mathbf{Q}} = \mathbf{I}_{M(K+\beta)} - \check{\mathbf{G}}\check{\mathbf{G}}^{\dagger}$. The projected received signal $\check{\mathbf{y}}'$ is given by

$$\check{\mathbf{y}}' \triangleq \check{\mathbf{Q}} \underbrace{\mathbf{A}\check{\mathbf{i}}_{\text{eqv}}}_{\triangleq \check{\mathbf{i}}} + \check{\mathbf{Q}}\check{\mathbf{n}} = \check{\mathbf{Q}}_{\text{eqv}}\check{\mathbf{i}}_{\text{eqv}} + \check{\mathbf{n}}' \tag{24}$$

where, $\check{\mathbf{i}}_{\text{eqv}} \triangleq \begin{bmatrix} \check{\mathbf{i}}_W^{(1)^T} & \dots & \check{\mathbf{i}}_W^{(K)^T} & \bar{\mathbf{i}}_P^{(1)^T} & \dots & \bar{\mathbf{i}}_P^{(\beta)^T} \end{bmatrix}^T$, $\check{\mathbf{n}}' \triangleq \check{\mathbf{Q}}\check{\mathbf{n}}$, and the *modified measurement matrix* $\check{\mathbf{Q}}_{\text{eqv}} \triangleq \check{\mathbf{Q}}\mathbf{A}$, where $\mathbf{A}$ is defined in (7).

Although the windowing operation enhances sparsity, we found that the OMP algorithm was not effective due to the power leakage caused by the CFO. Therefore, we instead estimate $\check{\mathbf{i}}_{\text{eqv}}$ by solving the following convex optimization problem using convex optimization techniques:

$$\hat{\check{\mathbf{i}}}_{\text{eqv}} \triangleq \underset{\mathbf{i}\in\mathbb{C}^{(K+\beta)M}}{\operatorname{argmin}} \|\mathbf{i}\|_1 \text{ subject to}$$
$$\|\check{\mathbf{Q}}_{\text{eqv}}\mathbf{i} - \check{\mathbf{y}}'\|_2^2 \le \epsilon_1 \quad \text{and} \quad \|\check{\mathbf{y}} - \mathbf{A}\mathbf{i}\|_2^2 \le \epsilon_2,$$

where ϵ_1 and ϵ_2 are set such that $\epsilon_1 \le \|\check{\mathbf{n}}'\|_2^2$ and $\epsilon_2 \le \|\check{\mathbf{G}}\mathbf{x} + \check{\mathbf{n}}\|_2^2$ with high probability. Note that, in contrast to (9), the sparsity level of NBI is unknown due to the power leakage. The constraint in OMP on the sparsity level $\|\mathbf{i}\|_0 = S$ is effectively replaced here by the absolute squared error, $\|\check{\mathbf{Q}}_{\text{eqv}}\mathbf{i} - \check{\mathbf{y}}'\|_2^2 \le \epsilon_1$. In addition, to further improve the $\check{\mathbf{i}}_{\text{eqv}}$ estimate, we have introduced an additional constraint on the received signal $\check{\mathbf{y}}$ (before nulling the information signal) based on (23), $\|\check{\mathbf{y}} - \mathbf{A}\mathbf{i}\|_2^2 \le \epsilon_2$. The estimated $\hat{\check{\mathbf{i}}}_{\text{eqv}}$ can now be used to find the support (non-zero indices) of $\check{\mathbf{i}}_{\text{eqv}}$. In particular, we compare the power of each element j of the vector $\hat{\check{\mathbf{i}}}_{\text{eqv}}$, determined by $\left|\hat{\check{\mathbf{i}}}_{\text{eqv}}[j]\right|^2$, with the average noise power per element, determined by $\frac{\max\{\epsilon_1,\epsilon_2\}}{(K+\beta)M)}$, to estimate the support vector I as follows:

$$I = \left\{ j : \left|\hat{\check{\mathbf{i}}}_{\text{eqv}}[j]\right|^2 > \frac{\max\{\epsilon_1,\epsilon_2\}}{(K+\beta)M)} \right\}. \tag{25}$$

IV. Sparsity-Based Joint Estimation of Contiguous NBI and IN

In this section, we propose a sparse recovery framework for estimating contiguous NBI and IN signals. In this case, both NBI and IN are modeled as block sparse vectors with few non-zero blocks, each block of a size d_X elements and $X \in \{W, P\}$. Here, the blocks' boundaries are assumed to be known and each non-zero block can only start at one of the following indices $\{1,\ d_X+1,\ 2d_X+1, ...,\ (\zeta_X-1)d_X+1\}$, where $\zeta_X = \frac{M}{d_X}$, $X \in \{W, P\}$. In addition, we make the assumption that the number of subcarriers per OFDM symbol, denoted M, is an integer multiple of the block size[3] d_X. Hence, $\mathbf{i}_W^{(k)}$ and $\bar{\mathbf{i}}_P^{(j)}$ can be decomposed into ζ_W and ζ_P blocks denoted by $\mathbf{i}_{W,b_W}^{(k)}$ and $\bar{\mathbf{i}}_{P,b_P}^{(j)}$, respectively, where $b_W \in \{1 \cdots \zeta_W\}$ and $b_P \in \{1 \cdots \zeta_P\}$, and can be written as follows:

$$\mathbf{i}_W^{(k)} = \Big[\underbrace{i_W^{(k)}[1] \ \cdots \ i_W^{(k)}[d_W]}_{\left(\mathbf{i}_{W,1}^{(k)}\right)^T} \ \cdots \ \underbrace{i_W^{(k)}[M-d_W+1] \ \cdots \ i_W^{(k)}[M]}_{\left(\mathbf{i}_{W,\zeta_W}^{(k)}\right)^T} \Big]^T, \tag{26}$$

$$\bar{\mathbf{i}}_P^{(j)} = \Big[\underbrace{\bar{i}_P^{(j)}[1] \ \cdots \ \bar{i}_P^{(j)}[d_P]}_{\left(\bar{\mathbf{i}}_{P,1}^{(j)}\right)^T} \ \cdots \ \underbrace{\bar{i}_P^{(j)}[M-d_P+1] \ \cdots \ \bar{i}_P^{(j)}[M]}_{\left(\bar{\mathbf{i}}_{P,\zeta_P}^{(j)}\right)^T} \Big]^T. \tag{27}$$

In particular, $\mathbf{i}_W^{(k)}$ and $\bar{\mathbf{i}}_P^{(j)}$ are block-sparse vectors and $\rho_{W,B}^{(k)} \triangleq \sum_{b_W=1}^{\zeta_W} \mathbf{1}\left\{\|\mathbf{i}_{W,b_W}^{(k)}\|_2\right\}$ and $\rho_{P,B}^{(j)} \triangleq \sum_{b_P=1}^{\zeta_P} \mathbf{1}\left\{\|\mathbf{i}_{P,b_P}^{(j)}\|_2\right\}$ count the number of non-zero blocks in $\mathbf{i}_W^{(k)}$ and $\bar{\mathbf{i}}_P^{(j)}$, respectively. The indicator function $\mathbf{1}\{.\}$ is equal to 1 for a non-zero argument and is 0 otherwise. For $d_W = d_P = 1$, $\rho_{W,B}^{(k)}$ and $\rho_{P,B}^{(j)}$ count the number of non-zero elements in $\mathbf{i}_W^{(k)}$ and $\bar{\mathbf{i}}_P^{(j)}$, respectively.

Following the same procedure in (6) through (8), the problem of contiguous NBI and IN recovery can be reduced to the estimation of a block sparse vector $\mathbf{i}_{\text{eqv}}$ with S_B non-zero entries, where $S_B \triangleq \sum_{k=1}^{K} \rho_{W,B}^{(k)} + \sum_{j=1}^{\beta} \rho_{P,B}^{(j)}$. Exploiting this block-sparse structure, we can estimate $\mathbf{i}_{\text{eqv}}$ from (8) by solving the following optimization problem [21]:

$$\hat{\mathbf{i}}_{\text{eqv}} \triangleq \underset{\mathbf{i}\in\mathbb{C}^{(K+\beta)M}}{\operatorname{argmin}} \sum_{l=1}^{M(\frac{K}{d_W}+\frac{\beta}{d_P})} \|\mathbf{i}_l\|_2, \text{ subject to } \|\mathbf{Q}_{\text{eqv}}\mathbf{i} - \mathbf{y}'\|_2^2 \leqslant \epsilon,$$

where $\mathbf{i}_l$ denotes the block number l in the vector $\mathbf{i}$.

As an alternative, several greedy algorithms from the CS literature can be applied to solve this problem efficiently. One example is the *block orthogonal matching pursuit* (BOMP) algorithm [21], which is an extension of the traditional OMP algorithm [24]. BOMP constructs the blocks of $\mathbf{i}_{\text{eqv}}$ iteratively by determining the sub-block of the measurement matrix $\mathbf{Q}_{\text{eqv}}$ that is most correlated with the measurements in (8) followed by solving the LS problem using the selected sub-blocks. These sub-blocks are constructed from the column vectors of $\mathbf{Q}_{\text{eqv}}$ with a size of $M(K+\beta) \times d$ each, where $d = \min\{d_W,\ d_P\}$, and $\mathbf{Q}_{\text{eqv}}$ is defined as follows:

$$\mathbf{Q}_{\text{eqv}} = \tag{28}$$
$$\Big[\underbrace{\mathbf{q}_{\text{eqv}}[1] \ \cdots \ \mathbf{q}_{\text{eqv}}[d]}_{\mathbf{Q}_{\text{eqv},1}} \ \cdots \ \underbrace{\mathbf{q}_{\text{eqv}}[M(K+\beta)-d+1] \ \cdots \ \mathbf{q}_{\text{eqv}}[M(K+\beta)]}_{\mathbf{Q}_{\text{eqv},\frac{M(K+\beta)}{d}}}\Big],$$

where $\mathbf{q}_{\text{eqv}}[b]$ denotes the b^{th} column of $\mathbf{Q}_{\text{eqv}}$. For completeness, we summarize the BOMP algorithm main steps in Algorithm 3 using the notation of this paper.

[3]When M is not an integer multiple of the block size d_X, the last few elements that form an incomplete block will not be considered as a block and, hence, will not be detected. In this case, $\zeta_X = \lfloor \frac{M}{d_X} \rfloor$, while everything else in the proposed framework still holds.

Algorithm 3 BOMP for Joint Estimation of Contiguous NBI and IN

Inputs: Matrix $\mathbf{Q}_{\text{eqv}}$, vector $\mathbf{y}'$, and block sparsity level S_B.
Initialization: Define set index $I_0 = \{\}$, set residual $\mathbf{r}_0 = \mathbf{y}'$, estimate $\hat{\mathbf{i}}_{\text{eqv}} = \mathbf{0}_{(K+\beta)M\times 1}$, and iteration count $l = 1$.
The l^{th} iteration:

1) Calculate $\delta_i = \| \left(\mathbf{Q}_{\text{eqv},i}\right)^H \mathbf{r}_{l-1} \|_2$ for all $i \notin I_{l-1}$.
2) Select index of the next non-zero block at the l^{th} iteration as $c_l = \underset{i}{\operatorname{argmax}}\ \delta_i$.
3) Update the non-zero blocks indices as $I_l = I_{l-1} \cup \{c_l\}$.
4) Solve the following optimization problem to find $\hat{\mathbf{i}}_{\text{eqv},l}(j)$ for $j \in I_l$:

$$\min_{\{\mathrm{i}(j)\}\in I_l} \left\| \mathbf{y}' - \sum_{j\in I_l} \mathbf{Q}_{\text{eqv},j}\mathrm{i}(j) \right\|_2 . \tag{29}$$

5) Calculate the residual error term in the l^{th} iteration as

$$\mathbf{r}_l = \mathbf{y}' - \sum_{j\in I_l} \mathbf{Q}_{\text{eqv},j}\hat{\mathbf{i}}_{\text{eqv},l}(j). \tag{30}$$

6) **If** $l = S_B$ then exit, **else** set $l = l+1$ and go to Step 1.

Note that in case of the size of the non-zero blocks d in the vector $\mathbf{i}_{\text{eqv}}$ is known but the boundaries of those blocks are not known, the BOMP performance will be significantly degraded because the modified measurement matrix $\mathbf{Q}_{\text{eqv}}$ cannot be partitioned into sub-matrices that are aligned perfectly with the blocks of $\mathbf{i}_{\text{eqv}}$. This challenge is investigated in the next section.

Next, for our proposed joint estimation of contiguous NBI and IN algorithm, we investigate the following extensions[4]. First, in Subsection IV-A, we consider the general problem of unknown NBI and IN bursts' boundaries. Second, in Subsection IV-B, we exploit knowledge of the second order statistics of NBI and IN to enhance their estimation for the contiguous NBI and IN sparse recovery problem. Finally, in Subsection IV-C, we exploit the high spatial correlation of the NBI and IN signals across different antennas/wires to convert a generally non-contiguous sparse recovery problem to a multi-level contiguous sparse recovery problem.

A. Joint Estimation of NBI-IN with Unknown Bursts' Boundaries

In this subsection, we relax our assumption of the *known blocks boundaries* and extend the recovery algorithm to cover the general case of *unknown bursts' boundaries*, i.e., the non-zero bursts of $\mathbf{i}_{\text{eqv}}$ may not align with the predefined sub-matrices of $\mathbf{Q}_{\text{eqv}}$ in (28). Instead, only the number of non-zero entries, denoted by S, and the number of bursts, denoted by $\mathcal{C}$, are assumed to be known.

In [22], a new CS recovery algorithm, called the $(S,\mathcal{C})$ algorithm, was introduced. The $(S,\mathcal{C})$ algorithm exploits the bursts' sparse structure without any prior knowledge of the bursts' boundaries, i.e., only knowledge of S and $\mathcal{C}$ is needed.

[4]We do not discuss the asynchronous case for the contiguous NBI and IN recovery problem since it is similar to the non-contiguous NBI and IN recovery problem.

The $(S,\mathcal{C})$ algorithm builds on the matching pursuit (CoSaMP) algorithm [26] with modified pruning based on dynamic programming principles. For completeness, we summarize the key steps of the $(S,\mathcal{C})$ algorithm in Algorithm 4 using the notation of this paper.

Algorithm 4 $(S,\mathcal{C})$ Algorithm for Joint Estimation of Contiguous NBI and IN with Unknown Bursts' Boundaries

Inputs: Matrix $\mathbf{Q}_{\text{eqv}}$, vector $\mathbf{y}'$, number of non-zero entries S, burst sparsity level $\mathcal{C}$ and the normalized difference between the estimated vector in two consecutive iterations, denoted by μ, where μ quantifies the performance-complexity trade-off (smaller μ results in better estimates with more iterations).
Initialization: Set residual $\mathbf{r}_0 = \mathbf{y}'$, estimate $\hat{\mathbf{i}}_{\text{eqv},0} = \mathbf{0}_{(K+\beta)M\times 1}$, and iteration count $l = 1$.
The l^{th} iteration:

1) Update the residual as $\mathbf{r}_l = \mathbf{y}' - \mathbf{Q}_{\text{eqv}}\hat{\mathbf{i}}_{\text{eqv},l-1}$.
2) Calculate $\mathbf{e} = \mathbf{Q}_{\text{eqv}}^H \mathbf{r}_l$.
3) Prune $\mathbf{e}$ using $|\mathbf{e}|$ to calculate the best $2S$ indices set $\mathbf{\Omega}$ for $2\mathcal{C}$ bursts based on the pruning algorithm in [22].
4) Form set $T = \mathbf{\Omega} \cup \text{supp}\left(\hat{\mathbf{i}}_{\text{eqv},l-1}\right)$, where $\text{supp}\left(\mathbf{x}\right)$ denotes indices of the non-zero entries of $\mathbf{x}$.
5) Define the vector $\mathbf{b} = \mathbf{0}_{(K+\beta)M\times 1}$ and estimate the elements in the set T by applying the LS estimator as follows: $\mathbf{b}(T) = \mathbf{Q}_{\text{eqv}}(:,T)^{\dagger}\mathbf{y}'$, where $\mathbf{Q}_{\text{eqv}}(:,T)$ is formed from the $\mathbf{Q}_{\text{eqv}}$ columns indexed by T.
6) Prune the vector $\mathbf{b}$ using the absolute values $|\mathbf{b}|$ to calculate the best S non-zero entries in $\mathcal{C}$ bursts and compute $\hat{\mathbf{i}}_{\text{eqv},l}$.
7) The stopping criterion will depend on the convergence of the estimated $\hat{\mathbf{i}}_{\text{eqv},l}$. **If** $\frac{\|\hat{\mathbf{i}}_{\text{eqv},l} - \hat{\mathbf{i}}_{\text{eqv},l-1}\|}{\|\hat{\mathbf{i}}_{\text{eqv},l}\|} \leq \mu$, **then** exit, **else** set $l = l+1$ and go to Step 1.

The main idea behind the pruning algorithm in [22] is to use dynamic programming principles to construct the bursts iteratively. In each pruning iteration, either new entries are added to the constructed bursts, or those bursts are split into more bursts until all of the S non-zero elements in the $\mathcal{C}$ bursts are calculated. The reader is referred to [22] for more details.

B. LMMSE Based BOMP

Similar to Subsection III-B, replacing LS with LMMSE in BOMP entails computing the covariance matrices of $\mathbf{i}_{\text{eqv}}$ and $\mathbf{n}'$. The noise covariance matrix $\mathbf{R}_{\mathbf{n}'}$ can be evaluated exactly as in (21). However, we need to derive the covariance matrix of $\mathbf{i}_{\text{eqv}}$, denoted $\tilde{\mathbf{R}}_{\mathbf{i}_{\text{eqv}}}$, and capture the sparsity profile of the contiguous NBI and IN vectors. Similar to Subsection III-B, since the NBI and IN vectors are assumed to be independent from each other and independent across the antennas/wires, the covariance matrix $\tilde{\mathbf{R}}_{\mathbf{i}_{\text{eqv}}}$ is a block diagonal matrix of submarices $\tilde{\mathbf{R}}^{(u)}_{\mathbf{i}_{\text{eqv}},X}$ as in (17). In addition, each submatrix $\tilde{\mathbf{R}}^{(u)}_{\mathbf{i}_{\text{eqv}},X}$ can be expressed as in (18). However, evaluation of the expression in (18) will be different here since the sparsity profile set for the block sparse NBI and IN, denoted by $\tilde{\mathfrak{U}_X}$, includes only the block sparse profiles which is different than the sparsity profile set of the non-contiguous sparse NBI and IN assumed

in Subsection III-B. In particular, assume that the NBI/IN blocks are of width $d_X,\ X \in \{W, P\}$, and assume d_X to be an odd number. The center of the block c is selected uniformly at random from all valid indices of the OFDM symbols which are given by the set $\{\frac{d_X-1}{2}+1, \frac{d_X-1}{2}+2, \cdots, M-\frac{d_X-1}{2}\}$. Note that indices less than $\frac{d_X-1}{2}+1$ and greater than $M-\frac{d_X-1}{2}$ are not valid indices for the center of block c since they can not construct a complete block. The probability density function (PDF) of activating the $\tilde{\omega_X}$ block in an OFDM symbol with M subcarriers can be defined by characterizing the PDF of the center of block which can be written as follows:

$$p(\tilde{\omega}_{c,X}) = \begin{cases} \frac{1}{\tilde{N}}, & \frac{d_X-1}{2} < c \leq M - \frac{d_X-1}{2}, \\ 0, & \text{otherwise}, \end{cases} \tag{31}$$

where c is the center index of the selected $\tilde{\omega}$ block and $\tilde{N} = M - d_X + 1$. Hence, each submatrix $\tilde{\mathbf{R}}^{(u)}_{\mathbf{i}_{\text{eqv}},X}$ can be evaluated as follows:

$$\tilde{\mathbf{R}}^{(u)}_{\mathbf{i}_{\text{eqv}},X} = \mathcal{E}_X \times \begin{cases} \frac{m}{\tilde{N}}, & 1 \leq m < d_X, \\ \frac{d_X}{\tilde{N}}, & d_X \leq m \leq M - d_X + 1, \\ \frac{\tilde{N}-d_X+1}{\tilde{N}}, & M - d_X + 1 < m \leq M. \end{cases} \tag{32}$$

C. Multi-Level BOMP

Here, we exploit the NBI and IN spatial correlation across the receive ports (either antennas or wires for the wireless or PLC systems, respectively) to convert the non-contiguous NBI and IN estimation problem to a block sparse recovery problem to enhance the estimation performance and/or reduce the complexity. In practice, the NBI tends to affect the same subcarriers over different receive antennas while the IN tends to occur at the same time samples on different receive wires. Thus, the NBI and IN signals share the same support indices over different antennas and wires, respectively.

In other words, although the problem formulation was originally non-contiguous (non-block sparse) NBI and IN recovery, we can convert it to a block sparse NBI and IN recovery problem by stacking the per subcarrier/time-sample received signal over the different antennas/wires. As a result, the non-block sparse NBI (in the frequency domain) will be converted to *block sparse* NBI with a block size equal to the number of antennas K. Similarly, the non-block sparse IN (in the time domain) will be converted to *block sparse* IN with a block size equal to the number of wires β. Moreover, we assume that NBI and IN affect the same subcarrier/samples indices over different antennas/wires which results in the same sparsity level for all antennas, i.e., $\rho^{(k)}_W = \rho_W$ for all $k \in \{1, ..., K\}$, and the same sparsity level for all wires, i.e., $\rho^{(j)}_P = \rho_P$ for all $j \in \{1, ..., \beta\}$. Hence, the problem can be considered as a *multi-level* block sparse recovery problem with only two block sizes K and β (since K and β are generally unequal), unlike the multi-level OMP recovery problem in Subsection III-A which assumed different sparsity levels for the different antennas/wires.

To reap the benefits of this spatial correlation in SIMO hybrid powerline-wireless transmission, we extend the conventional BOMP algorithm in [21] to support multiple block sparsity levels as described in the sequel.

Mathematically, in contrast to concatenating the FD received signals of the wireless and PLC links as shown in (5), here, we stack the FD wireless received signal on top of the TD PLC received signal as follows:

$$\underbrace{\begin{bmatrix} \mathbf{y}^{(1)}_W \\ \vdots \\ \mathbf{y}^{(K)}_W \\ \bar{\mathbf{y}}^{(1)}_P \\ \vdots \\ \bar{\mathbf{y}}^{(\beta)}_P \end{bmatrix}}_{\triangleq \tilde{\mathbf{y}}} = \underbrace{\begin{bmatrix} \Lambda^{(1)}_W \\ \vdots \\ \Lambda^{(K)}_W \\ \bar{\mathbf{H}}^{(1)}_P \mathbf{F}^H_M \\ \vdots \\ \bar{\mathbf{H}}^{(\beta)}_P \mathbf{F}^H_M \end{bmatrix}}_{\triangleq \tilde{\mathbf{G}}} \mathbf{x} + \underbrace{\begin{bmatrix} \mathbf{i}^{(1)}_W \\ \vdots \\ \mathbf{i}^{(k)}_W \\ \bar{\mathbf{i}}^{(1)}_P \\ \vdots \\ \bar{\mathbf{i}}^{(\beta)}_P \end{bmatrix}}_{\triangleq \tilde{\mathbf{i}}} + \underbrace{\begin{bmatrix} \mathbf{n}^{(1)}_W \\ \vdots \\ \mathbf{n}^{(K)}_W \\ \bar{\mathbf{n}}^{(1)}_P \\ \vdots \\ \bar{\mathbf{n}}^{(\beta)}_P \end{bmatrix}}_{\triangleq \tilde{\mathbf{n}}}. \tag{33}$$

Using the hybrid frequency-time domain structure in (33), the received signal samples can be permuted such that the NBI and IN vectors at particular subcarriers and time samples from different antennas and wires form blocks of size K and β, respectively. This can not be accomplished in the pure frequency-domain structure in (5) because of the DFT matrix multiplying the IN vector. In particular, the received signal samples are permuted as follows:

$$\underbrace{\begin{bmatrix} y^{(1)}_W[1] \\ \vdots \\ y^{(K)}_W[1] \\ \vdots \\ y^{(1)}_W[M] \\ \vdots \\ y^{(K)}_W[M] \\ \bar{y}^{(1)}_P[1] \\ \vdots \\ \bar{y}^{(\beta)}_P[1] \\ \vdots \\ \bar{y}^{(1)}_P[M] \\ \vdots \\ \bar{y}^{(\beta)}_P[M] \end{bmatrix}}_{\triangleq \tilde{\mathbf{r}}} = \underbrace{\begin{bmatrix} \mathbf{S}_W & \mathbf{0}_{\beta M \times \beta M} \\ \mathbf{0}_{KM \times KM} & \mathbf{S}_P \end{bmatrix}}_{\triangleq \mathbf{S}} \underbrace{\begin{bmatrix} y^{(1)}_W[1] \\ \vdots \\ y^{(1)}_W[M] \\ \vdots \\ y^{(K)}_W[1] \\ \vdots \\ y^{(K)}_W[M] \\ \bar{y}^{(1)}_P[1] \\ \vdots \\ \bar{y}^{(1)}_P[M] \\ \vdots \\ \bar{y}^{(\beta)}_P[1] \\ \vdots \\ \bar{y}^{(\beta)}_P[M] \end{bmatrix}}_{\triangleq \tilde{\mathbf{y}}}, \tag{34}$$

where $\mathbf{S}_W$ and $\mathbf{S}_P$ are permutation matrices. Note that in (34), the elements of vector $\tilde{\mathbf{r}}$ are arranged such that for each subcarrier, we stack the received samples of all antennas/wires together. In contrast, the elements of vector $\tilde{\mathbf{y}}$ are arranged such that for each antenna/wire, we stack all subcarriers together. From (33) and (34), we can write

$$\tilde{\mathbf{r}} = \mathbf{S}\tilde{\mathbf{y}} \triangleq \mathbf{S}\tilde{\mathbf{G}}\mathbf{x} + \mathbf{S}\tilde{\mathbf{i}} + \mathbf{S}\tilde{\mathbf{n}}. \tag{35}$$

Similar to (6), we null the desired signal by projecting $\tilde{\mathbf{r}}$ on to the left null space of $\mathbf{G}_{\text{eqv}} = \mathbf{S}\tilde{\mathbf{G}}$ to get

$$\mathbf{r}' \triangleq \tilde{\mathbf{Q}}_{\text{eqv}}\tilde{\mathbf{r}} = \tilde{\mathbf{Q}}_{\text{eqv}}\mathbf{S}\tilde{\mathbf{i}} + \tilde{\mathbf{n}}', \tag{36}$$

where $\tilde{\mathbf{Q}}_{\text{eqv}} = \mathbf{I}_{M(K+\beta)} - \mathbf{G}_{\text{eqv}}\mathbf{G}^{\dagger}_{\text{eqv}}$ and $\tilde{\mathbf{n}}' \triangleq \tilde{\mathbf{Q}}_{\text{eqv}}\mathbf{S}\tilde{\mathbf{n}}$.

Let $\tilde{\mathbf{i}}_{\text{eqv}} \triangleq \mathbf{S}\tilde{\mathbf{i}}$ denote the permuted version of the $\tilde{\mathbf{i}}$ vector. Since $\tilde{\mathbf{i}}_{\text{eqv}}$ is a block sparse vector, this reduces the problem of estimating $\tilde{\mathbf{i}}_{\text{eqv}}$ to a conventional block-sparse recovery problem with the main difference being that the sizes of the blocks are known but *not* equal. Consequently, we modify the conventional BOMP algorithm presented in [21] by dividing the measurement matrix $\tilde{\mathbf{Q}}_{\text{eqv}}$ into two submatrices to accommodate different block sizes as follows:

$$\tilde{\mathbf{Q}}_{\text{eqv}} = \left[\tilde{\mathbf{Q}}^{(W)}_{\text{eqv},1},\ \cdots,\ \tilde{\mathbf{Q}}^{(W)}_{\text{eqv},M},\ \tilde{\mathbf{Q}}^{(P)}_{\text{eqv},1},\ \cdots,\ \tilde{\mathbf{Q}}^{(P)}_{\text{eqv},M}\right],$$

where $\tilde{\mathbf{Q}}^{(W)}_{\text{eqv},i}$ and $\tilde{\mathbf{Q}}^{(P)}_{\text{eqv},i},\ i \in \{1,\ \cdots,\ M\}$ are submatrices that consist of K and β columns, respectively. Our proposed multi-level BOMP is summarized in Algorithm 5.

Algorithm 5 Multi-level BOMP for Joint Estimation of NBI and IN

Initialization: Define index set $\tilde{I}^{(W)}_0 = I^{(W)}_0 = \{\}$ and $\tilde{I}^{(P)}_0 = I^{(P)}_0 = \{\}$, set residual $\mathbf{r}_0 = \mathbf{r}'$, $\hat{\tilde{\mathbf{i}}}_{\text{eqv}} = \mathbf{0}_{(K+\beta)M}$, iteration count $l = 1$, and set $z_X = 0$ where $X \in \{W, P\}$.

The l^{th} iteration:

1) Compute $\delta^{(W)}_i = \|\mathbf{r}^H_{l-1}\tilde{\mathbf{Q}}^{(W)}_{\text{eqv},i}\|_2/\|\tilde{\mathbf{Q}}^{(W)}_{\text{eqv},i}\|$ and $\delta^{(P)}_j = \|\mathbf{r}^H_{l-1}\tilde{\mathbf{Q}}^{(P)}_{\text{eqv},j}\|_2/\|\tilde{\mathbf{Q}}^{(P)}_{\text{eqv},j}\|\ \forall\ i \notin I^{(W)}_{l-1}$ and $j \notin I^{(P)}_{l-1}$.
2) Find the index $c_W = \underset{i}{\text{argmax}}\ \delta^{(W)}_i$ and the index $c_P = \underset{j}{\text{argmax}}\ \delta^{(P)}_j$. **If** $\delta^{(W)}_{c_W} > \delta^{(P)}_{c_P}$, **then** $c_l = c_W$ and $X = W$, **else** $c_l = c_P$ and $X = P$. Update $z_X = z_X + 1$.
3) **If** $z_X > \rho_X$, **then** set $I^{(X)}_l = \{1,\ \cdots,\ M\}$ and go to Step 1, **else** proceed to the next step.
4) Update the indices of non-zero blocks as $I^{(X)}_l = I^{(X)}_{l-1} \cup \{c_l\}$ and $\tilde{I}^{(X)}_l = \tilde{I}^{(X)}_{l-1} \cup \{c_l\}$.
5) Construct the row block matrix $\tilde{\mathbf{Q}}_l$ from $\tilde{\mathbf{Q}}^{(W)}_{\text{eqv},i}$ and $\tilde{\mathbf{Q}}^{(P)}_{\text{eqv},j}$ indexed by $i \in \tilde{I}^{(W)}_l$ and $j \in \tilde{I}^{(P)}_l$, respectively. Compute $\hat{\tilde{\mathbf{i}}}_{\text{eqv}}(\Omega_l) = \left(\tilde{\mathbf{Q}}_l\right)^{\dagger}\mathbf{r}'$, where $\hat{\tilde{\mathbf{i}}}_{\text{eqv}}(\Omega_l)$ denotes the elements of $\hat{\tilde{\mathbf{i}}}_{\text{eqv}}$ that are indexed by Ω_l defined as $\{(i-1)K+1,\ \cdots,\ iK : i \in \tilde{I}^{(W)}_l\} \cup \{(j-1)\beta+1+KM,\ \cdots,\ j\beta+KM : j \in \tilde{I}^{(P)}_l\}$.
6) Calculate the residual error term at the l^{th} iteration as $\mathbf{r}_l = \mathbf{r}' - \tilde{\mathbf{Q}}_l\hat{\tilde{\mathbf{i}}}_{\text{eqv}}(\Omega_l)$ and set $z_X = z_X + 1$.
7) **If** $z_W > \rho_W$ and $z_P > \rho_P$, **then** exit, **else** go to Step 1.

Note that the complexity reduction in the multi-level BOMP algorithm is mainly due to converting the noncontiguous sparse problem (which can be solved using OMP algorithm) into a block sparse problem (which can be solved using BOMP algorithm). It is well known that BOMP algorithm complexity is much less than the OMP algorithm complexity. However, the multi-level block sizes in the multi-level BOMP algorithm are mainly to account for the general case where the number of antennas is different than the number of wires (i.e., $K \neq \beta$), not for complexity reduction.

V. Numerical Results

In this section, we investigate the performance of our proposed sparsity-based algorithms for joint NBI and IN mitigation in SIMO hybrid PLC-wireless links. Unless stated otherwise, we assume that $K = 3, \beta = 3$, $M = 64$, and our comparison is with respect to the benchmark of sparsity-based separate wireless and PLC receive signal processing. We assume wireless channel with a uniform power delay profile, $L_W = 8$, CIR taps are zero-mean complex Gaussian, and normalized powers; i.e. $\mathbb{E}\left[|\bar{\mathbf{h}}^{(k)H}_W\bar{\mathbf{h}}^{(k)}_W|^2\right] = 1,\ k \in \{1,2,3\}$. Moreover, we assume synchronous NBI where each NBI signal has a fixed width of 3 contiguous subcarriers, i.e., $\rho^{(k)}_W = \rho^{(k)}_{W,B} = 3,\ \forall\ k \in \{1,2,3\}$, and whose values are i.i.d. zero-mean complex Gaussian with fixed NBI-to-background Gaussian noise (NBI-GN) ratio, defined as $\frac{\mathbb{E}\left[\mathbf{i}^{(k)H}_W\mathbf{i}^{(k)}_W\right]}{\sigma^2_W} = \frac{\mathcal{E}_W}{\sigma^2_W},\ \forall\ k \in \{1,2,3\}$. This scenario is similar to a Bluetooth signal (with 1 MHz bandwidth) interfering with an IEEE 802.11n WLAN signal (with 20 MHz bandwidth) [27], and is important in practice due to the coexistence of Bluetooth and WLAN signals in the 2.4 GHz unlicensed frequency band.

Furthermore, we assume synchronous IN which spreads over 3 contiguous time samples[5], i.e., $\rho^{(j)}_P = \rho^{(j)}_{P,B} = 3,\ \forall\ j \in \{1,2,3\}$. Moreover, we assume a fixed IN-to-background Gaussian noise (IN-GN) ratio, defined as $\frac{\mathbb{E}\left[\mathbf{i}^{(j)H}_P\mathbf{i}^{(j)}_P\right]}{\sigma^2_P} = \frac{\mathcal{E}_P}{\sigma^2_P},\ j \in \{1,2,3\}$. In addition, we assume that each PLC CIR consists of two equal-power taps, i.e., $L_p = 2$, having uniformly-distributed phases and lognormal distributed magnitudes with standard deviations of 0.6 [3], [28]. Once again, we assume unit-power channels; i.e. $\mathbb{E}\left[|\bar{\mathbf{h}}^{(j)H}_P\bar{\mathbf{h}}^{(j)}_P|^2\right] = 1,\ \forall\ j \in \{1,2,3\}$. Finally, for simplicity, we assume that both the PLC and wireless links have the same signal to noise ratio (SNR), i.e. $\frac{\mathbb{E}\left[\mathbf{x}^H\mathbf{x}\right]}{\sigma^2_W} = \frac{\mathbb{E}\left[\mathbf{x}^H\mathbf{x}\right]}{\sigma^2_P}$, although they could be different in practice.

In Fig. 2, we compare the bit error rate (BER) of four scenarios to quantify the performance gain of joint over separate processing in the presence of non-contiguous NBI and IN. In the first scenario, the NBI and IN signals are treated as noise and maximum ratio combining (MRC) is used to combine the received wireless and PLC signals. The second scenario corresponds to separate processing where the receiver of each link individually estimates and cancels the non-contiguous NBI and IN followed by MRC to combine both signals. Since it is shown in [11], [20] that sparsity-based techniques outperform traditional NBI and IN mitigation techniques, the second scenario corresponds to sparsity-based individual NBI and IN estimation. Fig. 2 demonstrates that the NBI/IN signals cannot be completely canceled in the second scenario and the residual NBI/IN signals result in an error floor. The third scenario represents the case of NBI and IN mitigation using our proposed method which can eliminate the error floor of [11], [20]. More specifically, our proposed method approaches the performance of the fourth scenario that corresponds to NBI-free and IN-free links. Next, we quantify the performance gains of joint processing over separate processing in Fig. 3. This figure shows the BER as

[5]Note that since the contiguous NBI/IN is a special case of non-contiguous NBI/IN, we can test the performance of the proposed non-contiguous sparse recovery techniques on the assumed contiguous NBI/IN, i.e., non contiguous NBI/IN techniques will not exploit the fact that NBI and IN are contiguous.

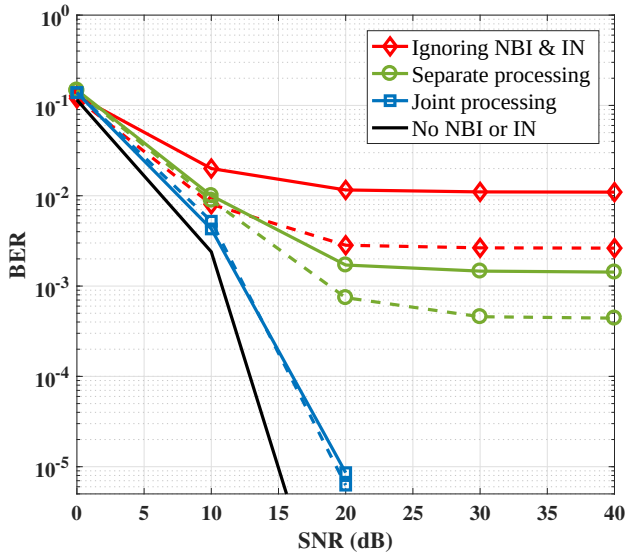

Fig. 2. BER performance for non-contiguous NBI and IN with $R = 4$ bits/sec/Hz with solid and dashed lines for S-NBI and S-IN ratios equal to -10 dB and -5 dB, respectively.

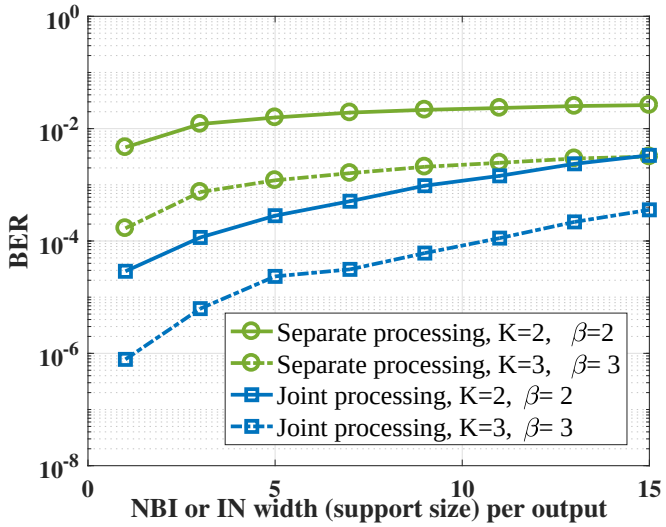

Fig. 3. BER performance for non-contiguous NBI and IN with S-NBI and S-IN equal to -5 dB while SNR=20 dB, and $R = 4$ bits/sec/Hz.

a function of the NBI and IN widths per receive signal port, which we are assume to be the same at each antenna/wire. Increasing the NBI and/or IN widths results in a higher BER since the sparsity is reduced. However, joint processing still outperforms separate processing significantly in this reduced-sparsity setting.

In Fig. 4, we investigate the performance of the multi-level OMP algorithm presented in Subsection III-A to exploit apriori knowledge of the sparsity level at each receive antenna and wire. It is clear that multi-level OMP achieves the same performance as OMP with much lower complexity by reducing the search space as discussed in Subsection III-A. In Fig. 5, we plot the computational complexity saving ratio of the multi-level OMP algorithm relative to the OMP complexity as a function the ratio ρ/M. The complexity ratio for the best and worst cases of the multi-level OMP algorithm are defined as $\frac{\mathbb{C}_{MOMP,b}-\mathbb{C}_{OMP}}{\mathbb{C}_{OMP}} \times 100$ and $\frac{\mathbb{C}_{MOMP,w}-\mathbb{C}_{OMP}}{\mathbb{C}_{OMP}} \times 100$. The quantities $\mathbb{C}_{OMP}$, $\mathbb{C}_{MOMP,b}$ and $\mathbb{C}_{MOMP,w}$ are computed using (13), (14) and (15), respectively. As shown in Fig. 5, for very small values of ρ/M, the worst and best cases achieve the

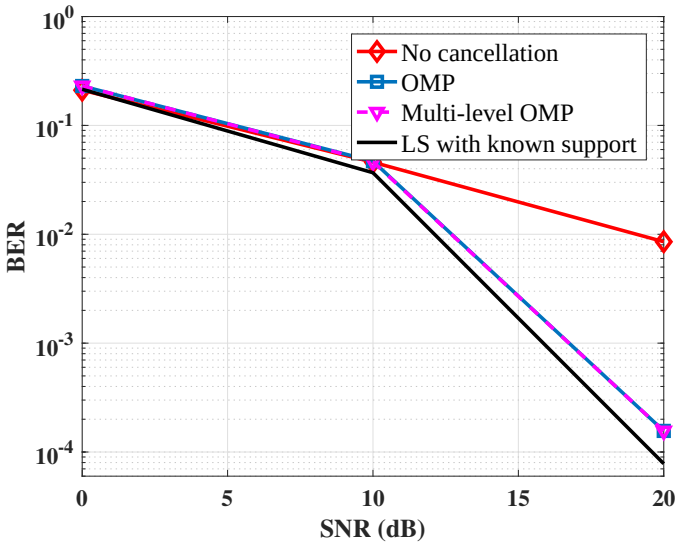

Fig. 4. BER performance versus SNR for $R = 6$ bits/sec/Hz and NBI-S=IN-S=3 dB using the modified multi-level OMP recovery algorithm for 3 antennas and 3 wires hybrid wireless-PLC system.

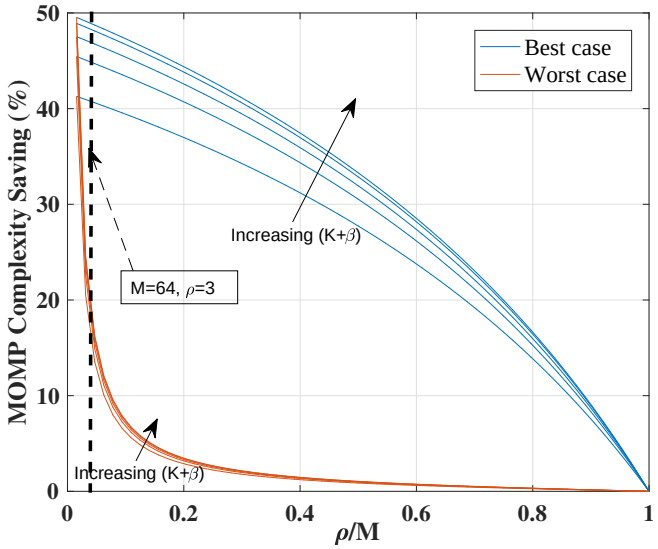

Fig. 5. Computational savings in multi-level OMP relative to OMP as a function of the ratio ρ/M.

same complexity reduction of close to 50%. In practice, this ratio ρ/M is expected to be small (less than 0.1) as shown in Fig. 6. For the parameters' default settings given in this section ($\rho = 3$, $M = 64$ and $K + \beta = 6$), the best case complexity reduction is 40% while the worst-case complexity reduction is 15%. Moreover, in Fig. 6, we show the complexity reduction calculated based on simulation of the multi-level OMP over the SNR range of $(0 : 40$ dB). As shown in Fig. 6, the complexity reduction based on simulations is bounded by the best and worst cases' curves computed based on our derived mathematical expressions. Furthermore, we can see that the complexity is slightly reduced with increasing $K + \beta$.

In Fig. 7, we examine the effect of Hamming windowing under asynchronous NBI[6] with CFO that is uniformly-distributed as defined in Subsection II. In addition, assuming that the NBI and IN bursts have the same width of 3, we set NBI-GN=IN-GN, and we use the proposed algorithm in Section III-C. As

[6]Note that all simulation results assume synchronous NBI and IN except Fig. 7 which assumes asynchronous NBI.

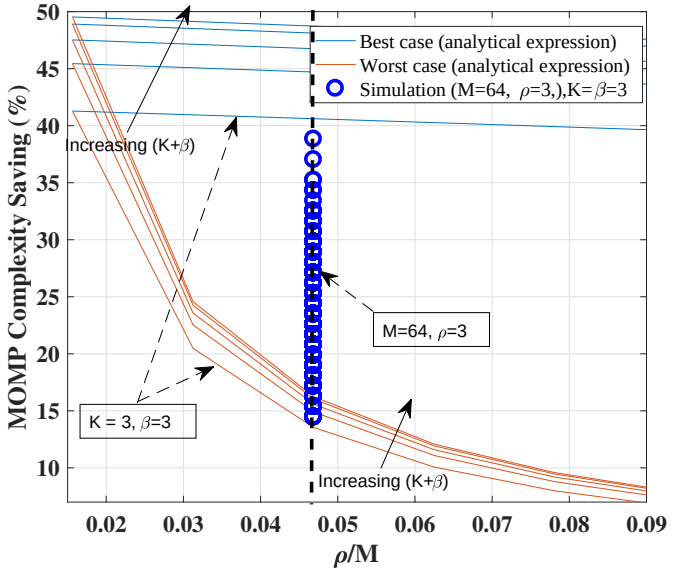

Fig. 6. A zoomed view of computational savings in multi-level OMP relative to OMP as a function of the ratio ρ/M.

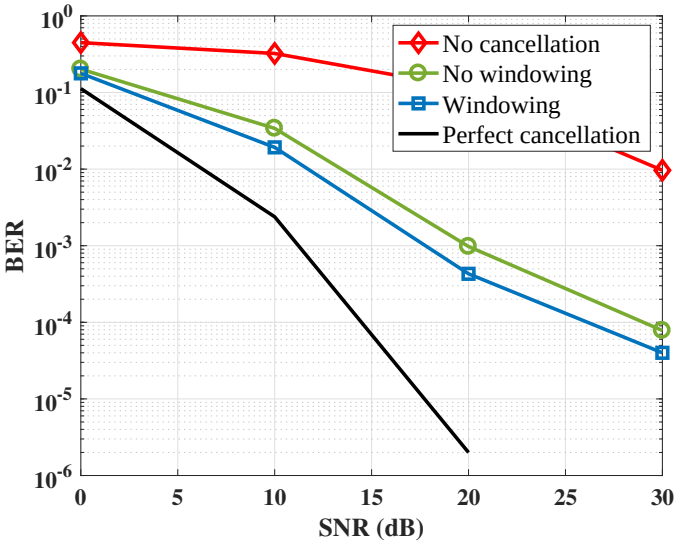

Fig. 7. BER performance versus SNR for $R = 4$ bits/sec/Hz and NBI-GN=IN-GN=40 dB using the CS recovery algorithm in Section III-C.

illustrated in this figure, the weaker the desired signal is, the higher is the performance gain due to windowing since the NBI effect becomes more pronounced. Furthermore, the BER simulations show up to 3 dB SNR gain at BER = 5×10^{-4} due to time-domain windowing.

To study the performance of the block-sparse recovery algorithms, we set the number of PLC and wireless receive ports to $K = \beta = 1$ to isolate any performance gain due to the processing of multiple receive signals. In Fig. 8, we use the performance metric of *average error vector magnitude* (AEVM), which we define as $\eta \triangleq \frac{\sum_{u=1}^{U} \|\mathbf{i}_{\text{eqv}} - \hat{\mathbf{i}}_{\text{eqv}}\|_2^2}{\sum_{u=1}^{U} \|\mathbf{i}_{\text{eqv}}\|_2^2}$ with U denoting the number of channel realizations ($U = 5000$ in these experiments). Note that a smaller value of η indicates better estimation performance. As a performance lower bound, we show the (ideal) LS performance assuming that the locations of the non-zero elements in the sparse IN and NBI vectors are perfectly known. We assume that the NBI and IN bursts have the same width of 5 and can occur anywhere within the OFDM symbol, i.e., we do not know the locations of the

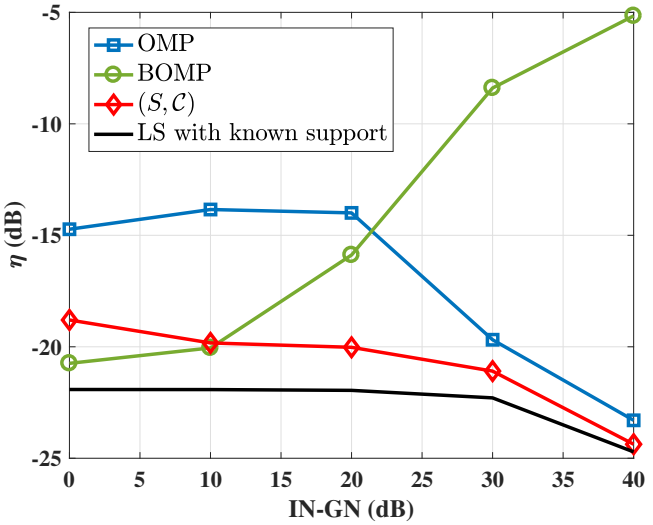

Fig. 8. AEVM versus IN-GN with NBI-GN=40dB for SISO systems. Here, NBI and IN bursts are assumed to be of width 5.

burst boundaries. For BOMP, we have a mismatch between the bursts' boundaries and the predefined sub-matrices of $\mathbf{Q}_{\text{eqv}}$ in (28). As Fig. 8 shows, the BOMP performance is significantly degraded when compared with the performance of the OMP and $(S, \mathcal{C})$ algorithms and this degradation increases as the IN-GN level increases. Moreover, the $(S, \mathcal{C})$ algorithm outperforms the traditional OMP algorithm over the entire IN-GN range. At high IN-GN levels, the performance gap between the $(S, \mathcal{C})$ and the traditional OMP algorithm diminishes because the higher power levels of the NBI and IN signals (relative to the thermal noise power level) enable accurate sparse recovery using both algorithms without the need for exploiting the bursty nature of the NBI and IN signals. Furthermore, the performances of both algorithms approach the ideal LS lower bound.

To further quantify the performance gain realized by exploiting the block-sparse structure, Fig. 9 compares the BERs of the aforementioned joint NBI/IN estimation algorithms. The $(S, \mathcal{C})$ algorithm achieves more than 2 dB and 5 dB SNR gain at BER=10^{-4} over the traditional OMP and BOMP algorithms, respectively. In addition, as SNR increases, the $(S, \mathcal{C})$ algorithm's performance approaches the LS performance assuming perfect knowledge of NBI and IN locations. Fig. 10 shows the BER performance for the case of a more generic scenario where the NBI and IN bursts have different widths of 3 and 5, respectively. Here, the performance gain of the $(S, \mathcal{C})$ algorithm over the BOMP algorithm is higher compared to the equal-width scenario in Fig. 9. For example, at BER =10^{-3}, an SNR gain of 5 dB is achieved for different-width NBI and IN bursts while only a gain of 2.5 dB is achieved when the NBI and IN bursts have the same width.

In Fig. 11, we plot the BER versus SNR for a fixed signal-to-NBI (S-NBI) and signal-to-IN (S-IN) ratios, defined as $\frac{\mathbb{E}[\mathbf{x}^H \mathbf{x}]}{\mathbb{E}[\mathbf{i}_W^{(k)H} \mathbf{i}_W^{(k)}]}$ and $\frac{\mathbb{E}[\mathbf{x}^H \mathbf{x}]}{\mathbb{E}[\mathbf{i}_P^{(j)H} \mathbf{i}_P^{(j)}]}$ $\forall\ k, j \in \{1, 2, 3\}$, respectively, equal to -3 dB. In this figure, we exploit the fact that NBI and IN share the same support set over different antennas and wires, respectively, for the case of 3 antennas and 2 wires. It is evident that the proposed multi-level BOMP algorithm in Subsection IV-C results in significant performance gain to the

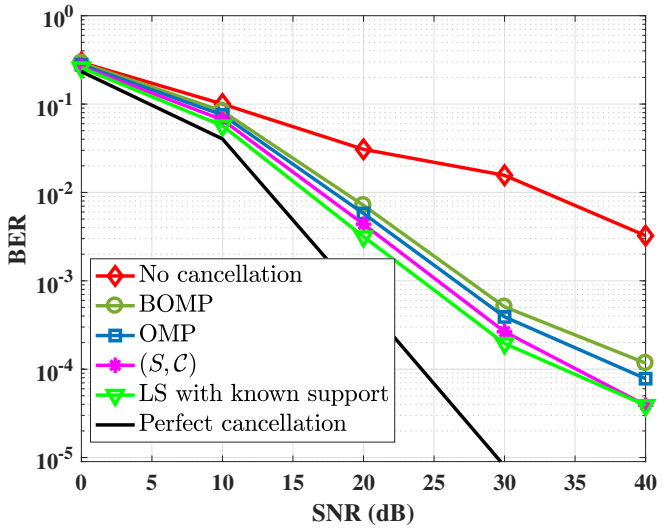

Fig. 9. BER performance versus SNR for $R = 4$ bits/sec/Hz, NBI-GN=40 dB and IN-GN=20 dB. Both NBI and IN have the same width of 5.

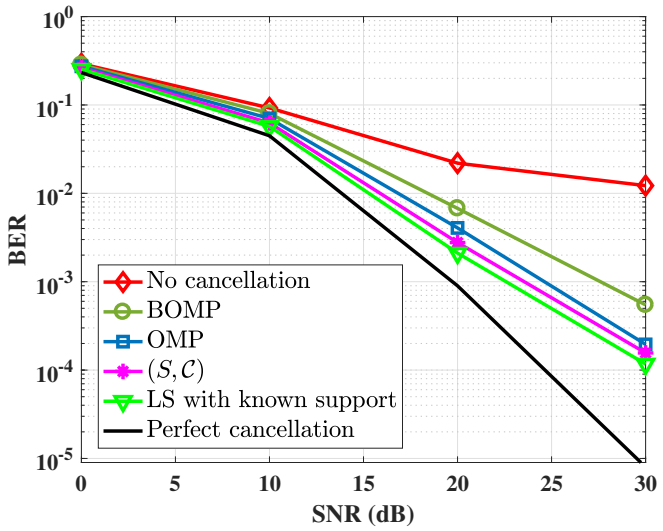

Fig. 10. BER performance versus SNR for $R = 4$ bits/sec/Hz, NBI-GN=40 dB and IN-GN=20 dB, with NBI and IN widths of 3 and 5, respectively.

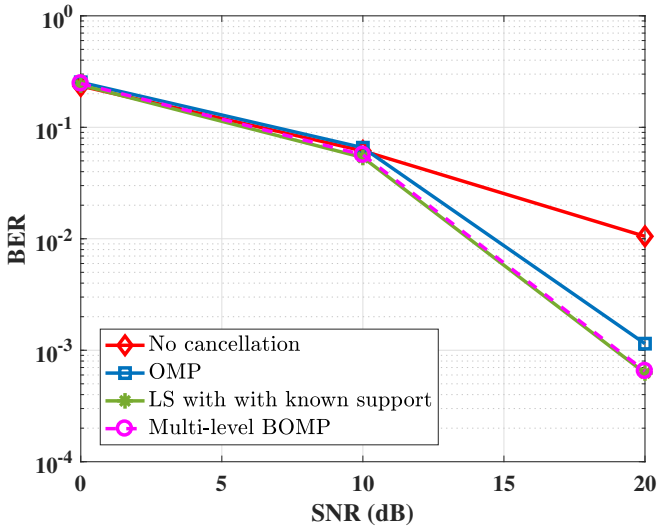

Fig. 11. BER versus SNR for $R = 6$ bits/sec/Hz, S-IN=S-NBI=-3 dB and $K = 3$ and $\beta = 2$.

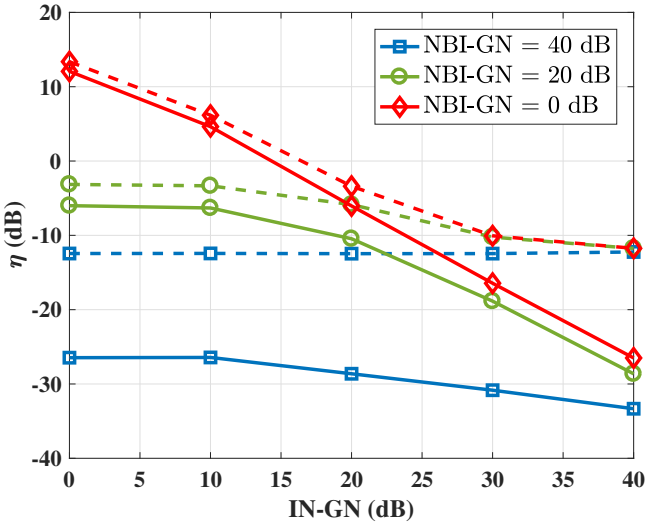

Fig. 12. AEVM for non-contiguous NBI and IN with joint (solid lines) and separate (dashed lines) processing for different NBI-GN and IN-GN levels.

extent that it approaches the LS with known support indices.

In Fig. 12, we show η for both joint (our proposed approach) and separate processing for different non-contiguous NBI-GN and IN-GN levels. We make the following two conclusions based on this figure. First, the higher the NBI-GN and IN-GN levels are, the better the estimation performance of both joint and separate processing will be. Second, our proposed joint processing always results in better performance than separate processing.

Finally, in Fig. 13, we examine the effect of replacing LS with LMMSE on the performance of the OMP algorithm. We plot BER for a 3-antenna and 3-wire system versus the NBI-GN and IN-GN levels that are assumed to be equal. For weak NBI and IN, we observe significant performance improvement over OMP and LS due to apriori knowledge about the NBI and IN statistics.

VI. Conclusion

We proposed a new framework to model and jointly estimate and mitigate non-contiguous and contiguous NBI and IN in SIMO hybrid PLC-wireless transmissions by exploiting their sparsity in the frequency and time domains, respectively. To enhance the sparse estimation performance, we investigated several NBI and IN properties and compared sparse recovery algorithms that can effectively exploit them.

Specifically, for non-contiguous NBI and IN, studied the practical scenario of asynchronous NBI and investigated the application of time-domain windowing to enhance the NBI's sparsity level and, hence, improve performance of sparsity-based NBI signal estimation. In addition, we exploited prior knowledge of the generally unequal sparsity levels at different antennas and wires and developed a multi-level OMP algorithm to further reduce the complexity of the sparse recovery algorithm.

For contiguous NBI and IN, the presented joint NBI and IN mitigation framework exploits their inherent block sparsity with or without knowledge of the bursts' boundaries. Moreover, we exploited the spatial correlation across the receive antennas and across the three-phase powerlines to convert the non-contiguous NBI and IN problem to a block sparse NBI and IN problem, after which we proposed a multi-level BOMP algorithm that can efficiently exploit the new block-sparse

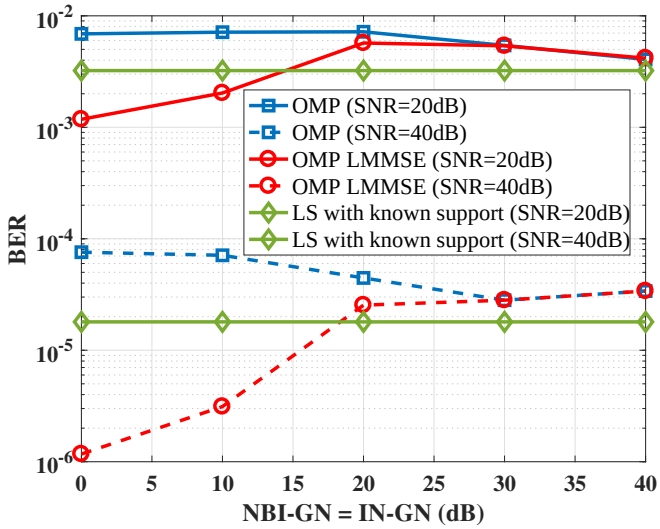

Fig. 13. BER versus NBI and IN power for $R = 4$ bits/s/Hz.

structure.

For both contiguous and non-contiguous NBI and IN with known second-order statistics, we quantified the performance gains of LMMSE-based sparse recovery algorithms over the conventional LS-based recovery of joint NBI and IN with known support indices. Finally, we quantified the NBI/IN mitigation performance gains of the investigated algorithms through extensive simulations and demonstrated the superiority of the joint PLC-wireless processing approach over PLC-only or wireless-only processing approaches.

REFERENCES

[1] M. Mokhtar, W. U. Bajwa, M. Elgenedy, and N. Al-Dhahir, "Exploiting Block Sparsity for Joint Mitigation of Asynchronous NBI and IN in Hybrid Powerline-Wireless Communications," in *Proc. IEEE International Conference on Smart Grid Communications (SmartGridComm)*, Nov 2015, pp. 362–367.

[2] M. Mokhtar, W. U. Bajwa, and N. Al-Dhahir, "Sparsity-aware joint narrowband interference and impulse noise mitigation for hybrid powerline-wireless transmission," in *Proc. IEEE Wireless Communications and Networking Conference (WCNC)*, March 2015, pp. 615–620.

[3] S. Guzelgoz, H. Celebi, and H. Arslan, "Analysis of a MultiChannel Receiver: Wireless and PLC Reception," in *Proc. EUSIPCO*, Aug. 2010, pp. 1106–1110.

[4] S. Lai and G. Messier, "Using the Wireless and PLC Channels for Diversity," *IEEE Trans. Commun.*, pp. 3865–3875, Dec 2012.

[5] S. W. Lai, N. Shabehpour, G. G. Messier, and L. Lampe, "Performance of Wireless/Power Line Media Diversity in the Office Environment," in *Proc. IEEE Global Communications Conference*, Dec 2014, pp. 2972–2976.

[6] J. H. Lee and Y. H. Kim, "Diversity relaying for parallel use of power-line and wireless communication networks," *IEEE Transactions on Power Delivery*, vol. 29, no. 3, pp. 1301–1310, June 2014.

[7] G. Sebaali and B. L. Evans, "Design tradeoffs in joint powerline and wireless transmission for smart grid communications," in *Proc. IEEE International Symposium on Power Line Communications and Its Applications (ISPLC)*, March 2015, pp. 83–88.

[8] "IEEE P1901.2/D0.11.00 draft standard for low frequency (less than 500 kHz) narrow band power line communications for Smart Grid applications," *Institute of Electrical and Electronics Engineers (IEEE) Standards Association*, August 2013.

[9] V. Oksman and J. Zhang, "G.HNEM: The New ITU-T Standard on Narrowband PLC Technology," *IEEE Comm. Mag.*, pp. 36–44, Dec. 2011.

[10] H. Ferreira, L. Lampe, J. Newbury, and T. Swart, *Power Line Communications: Theory and Applications for Narrowband and Broadband Communications over Power Lines*. John Wiley & Sons, 2010.

[11] A. Gomaa and N. Al-Dhahir, "A Sparsity-Aware Approach for NBI Estimation in MIMO-OFDM," *IEEE Trans. Wireless Comm.*, pp. 1854–1862, Jun. 2011.

[12] M. Sayed and N. Al-Dhahir, "Narrowband-PLC/wireless diversity for smart grid communications," in *Proc. IEEE GLOBECOM*, Austin, TX, 2014, pp. 2966–2971.

[13] M. Sayed, G. Sebaali, B. L. Evans, and N. Al-Dhahir, "Efficient diversity technique for hybrid narrowband-powerline/wireless smart grid communications," in *Proc. IEEE SmartGridComm*, Miami, FL, Nov. 2015, pp. 1–6.

[14] M. Sayed, T. A. Tsiftsis, and N. Al-Dhahir, "On the diversity of hybrid narrowband-plc/wireless communications for smart grids," *IEEE Transactions on Wireless Communications*, vol. 16, no. 7, pp. 4344–4360, July 2017.

[15] M. Sayed, A. E. Shafie, M. Elgenedy, R. C. Chabaan, and N. Al-Dhahir, "Enhancing the reliability of two-way vehicle-to-grid communications," in *Proc. IEEE Intelligent Vehicles Symposium (IV)*, June 2017, pp. 1922–1927.

[16] M. Sayed and N. Al-Dhahir, "Differential modulation diversity combining for hybrid narrowband-powerline/wireless smart grid communications," in *Proc. IEEE Global Conference on Signal and Information Processing (GlobalSIP)*, Dec 2016, pp. 876–880.

[17] M. Katayama, T. Yamazato, and H. Okada, "A mathematical model of noise in narrowband power line communication systems," *IEEE Journal on Selected Areas in Communications*, vol. 24, no. 7, pp. 1267–1276, 2006.

[18] M. Nassar, A. Dabak, I. H. Kim, T. Pande, and B. L. Evans, "Cyclostationary noise modeling in narrowband powerline communication for smart grid applications," in *Proc. IEEE ICASSP*, Kyoto, Japan, Mar. 2012, pp. 3089–3092.

[19] M. Elgenedy, M. Sayed, A. El Shafie, I. H. Kim, and N. Al-Dhahir, "Cyclostationary Noise Modeling Based on Frequency-Shift Filtering in NB-PLC," in *Proc. IEEE Globecom*, Washington, DC, Dec. 2016, pp. 1–6.

[20] G. Caire, T. Al-Naffouri, and A. Narayanan, "Impulse Noise Cancellation in OFDM: An Application of Compressed Sensing," in *Proc. IEEE Intl. Symp. Information Theory (ISIT)*, Jul. 2008, pp. 1293–1297.

[21] Y. Eldar, P. Kuppinger, and H. Bolcskei, "Block-Sparse Signals: Uncertainty Relations and Efficient Recovery," *IEEE Transactions on Signal Processing*, vol. 58, no. 6, pp. 3042–3054, June 2010.

[22] V. Cevher, P. Indyk, C. Hegde, and R. G. Baraniuk, "Recovery of Clustered Sparse Signals from Compressive Measurements ," in *Proc. Int. Conf. Sampling Theory Applicat. (SAMPTA), May 2009*.

[23] E. Candes, J. Romberg, and T. Tao, "Stable Signal Recovery from Incomplete and Inaccurate Measurements," *Comm. Pure App. Math.*, vol. 59, no. 9, pp. 1207–1223, Mar 2006.

[24] Y. Pati, R. Rezaiifar, and P. Krishnaprasad, "Orthogonal Matching Pursuit: Recursive Function Approximation with Applications to Wavelet Decomposition," in *Proc. Asilomar Conf. Sig., Syst. and Comp.*, 1993, pp. 40–44.

[25] S. M. Kay, *Fundamentals Of Statistical Signal Processing: Estimation Theory*. Prentice Hall, 1993.

[26] D. Needell and J. Tropp, "CoSaMP: Iteative Signal Recovery from Incomplete and Inaccurate Samples," *Appl. Computat. Harmon. Anal.*, vol. 26, no. 3, pp. 301–321, May 2009.

[27] E. Perahia and R. Stacey, *Next Generation Wireless LANs*. Cambridge University Press, 2013.

[28] S. Galli, "A Novel Approach to the Statistical Modeling of Wireline Channels," *IEEE Trans. Commun.*, pp. 1332–1345, May 2011.

Mahmoud Elgenedy received his B.Sc. and M.Sc. degrees in electrical engineering in 2005 and 2010, respectively, from Cairo University, Egypt. He is currently working towardshis Ph.D. degree in Electrical Engineeringat the University of Texas at Dallas, Richardson, TX, USA. From 2005 to 2007 he worked at SySDSoft (acquired by Intel Corp.) as a communication system design engineer. From 2008 to 2010 he worked on developing military standards modems at MTSE, Cairo, Egypt. From 2010 to 2014 he worked on the development of the LTE-UEat Wasiela,Cairo, Egypt. During summer 2015, he worked as an intern system design engineer at Broadcom Corp., Irvine, CA. He worked as an intern firmware design engineer at Qualcomm Corp., Boston, MA during the summer of 2017.

Mohamed Mokhtar Awadin is currently a senior 5G standards engineer at InterDigital, Inc. He received BSc degree in electronics and communications engineering from Alexandria University, Egypt, in 2008 and the MSc from Nile University, Egypt, in 2010. He earned his PhD degree in Electrical Engineering from University of Texas at Dallas, Richardson, TX, USA, in 2014. His research interests include cooperative communication and RF impairments equalization at the baseband.

Ridha Hamila received the Master of Science, Licentiate of Technology with distinction, and Doctor of Technology degrees from Tampere University of Technology (TUT), Department of Information Technology, Tampere, Finland, in 1996, 1999, and 2002, respectively. He is currently an Associate Professor at the Department of Electrical Engineering, Qatar University, Qatar. Also, he is adjunct Professor at the Department of Communications Engineering of TUT. From 1994 to 2002 he held various research and teaching positions at TUT within the Department of Information Technology, Finland. From 2002 to 2003 he was a System Specialist at Nokia research Center and Nokia Networks, Helsinki. From 2004 to 2009 he was with Etisalat University College, Emirates Telecommunications Corporation, UAE. His current research interests include mobile and broadband wireless communication systems, cellular and satellites-based positioning technologies, synchronization and DSP algorithms for flexible radio transceivers. In these areas, he has published over 60 journal and conference papers most of them in the peered reviewed IEEE publications, led two patents, and wrote numerous confidential industrial research reports. He has been involved in several past and current industrial projects Qtel, QNRF, Finnish Academy projects, TEKES, Nokia, EU research and education programs. He supervised a large number of under/graduate students and postdoctoral fellows.

Waheed U. Bajwa received BE (with Honors) degree in electrical engineering from the National University of Sciences and Technology, Pakistan in 2001, and MS and PhD degrees in electrical engineering from the University of Wisconsin-Madison in 2005 and 2009, respectively. He was a Postdoctoral Research Associate in the Program in Applied and Computational Mathematics at Princeton University from 2009 to 2010, and a Research Scientist in the Department of Electrical and Computer Engineering at Duke University from 2010 to 2011. He is currently an Associate Professor in the Department of Electrical and Computer Engineering at Rutgers University. His research interests include statistical signal processing, high-dimensional statistics, machine learning, networked systems, and inverse problems.

Dr. Bajwa has received a number of awards in his career including the Best in Academics Gold Medal and Presidents Gold Medal in Electrical Engineering from the National University of Sciences and Technology (2001), the Morgridge Distinguished Graduate Fellowship from the University of Wisconsin-Madison (2003), the Army Research Office Young Investigator Award (2014), the National Science Foundation CAREER Award (2015), Rutgers Universitys Presidential Merit Award (2016), Rutgers Engineering Governing Council ECE Professor of the Year Award (2016, 2017), and Rutgers Universitys Presidential Fellowship for Teaching Excellence (2017). He is a co-investigator on the work that received the Cancer Institute of New Jerseys Gallo Award for Scientific Excellence in 2017, a co-author on papers that received Best Student Paper Awards at IEEE IVMSP 2016 and IEEE CAMSAP 2017 workshops, and a Member of the Class of 2015 National Academy of Engineering Frontiers of Engineering Education Symposium. He served as an Associate Editor of the IEEE Signal Processing Letters (2014 2017), co-guest edited a special issue of Elsevier Physical Communication Journal on Compressive Sensing in Communications (2012), co-chaired CPSWeek 2013 Workshop on Signal Processing Advances in Sensor Networks and IEEE GlobalSIP 2013 Symposium on New Sensing and Statistical Inference Methods, and served as the Publicity and Publications Chair of IEEE CAMSAP 2015 and General Chair of the 2017 DIMACS Workshop on Distributed Optimization, Information Processing, and Learning. He is currently Technical Co-Chair of the IEEE SPAWC 2018 Workshop, a Senior Member of the IEEE, and serves on the MLSP, SAM, and SPCOM Technical Committees of the IEEE Signal Processing Society.

Ahmed S. Ibrahim is currently an assistant professor at the Electrical and Computer Engineering Department at Florida International University (FIU), Miami, FL, USA. He received the B.S. (with highest honors) and M.S. degrees in electronics and electrical communications engineering from Cairo University, Cairo, Egypt, in 2002 and 2004, respectively. He received the Ph.D. degree in electrical engineering from the University of Maryland, College Park, MD, USA, in 2009. Prior to joining FIU, Dr. Ibrahim was an assistant professor at Cairo University, wireless research scientist at Intel Corporation, and senior engineer at Interdigital Communications Inc. Dr. Ibrahims research interests span various topics of next generation mobile communications and Internet of Things such as heterogeneous networks, drone-assisted millimeter wave communications, and vehicular networks.

Naofal Al-Dhahir is Erik Jonsson Distinguished Professor at UT-Dallas. He earned his PhD degree in Electrical Engineering from Stanford University. From 1994 to 2003, he was a principal member of the technical staff at GE Research and AT&T Shannon Laboratory. He is co-inventor of 41 issued US patents, co-author of over 380 papers and co-recipient of 4 IEEE best paper awards. He is the Editor-in-Chief of IEEE Transactions on Communications and an IEEE Fellow.